Marine Geology 272 (2010) 285–306

Contents lists available at ScienceDirect

Marine Geology

journal homepage: www.elsevier.com/locate/margeo

Geological imprint of methane seepage on the seabed and biota of the convergent Hikurangi Margin, New Zealand: Box core and grab carbonate results

Kathleen A. Campbell [a,*], Campbell S. Nelson [b], Andrea C. Alfaro [c], Sheree Boyd [c], Jens Greinert [d,e], Stephanie Nyman [b,1], Emmanuelle Grosjean [f], Graham A. Logan [f], Murray R. Gregory [a], Steve Cooke [b], Peter Linke [g], Sophie Milloy [a], Irene Wallis [a]

[a] School of Environment, University of Auckland, Private Bag 92019, Auckland 1142, New Zealand
[b] Department of Earth and Ocean Sciences, University of Waikato, Private Bag 3105, Hamilton 3240, New Zealand
[c] School of Applied Sciences, Faculty of Health and Environmental Sciences, Auckland University of Technology, Private Bag 92006, Auckland 1142, New Zealand
[d] Royal Netherlands Institute for Sea Research (NIOZ), P.O. Box 59, 1790 AB Den Burg (Texel), The Netherlands
[e] Renard Centre of Marine Geology (RCMG), Ghent University, Krijgslaan 281 s.8, B-9000 Gent, Belgium
[f] Geoscience Australia, GPO Box 378, Canberra ACT 2601, Australia
[g] IFM-GEOMAR, Leibniz Institute of Marine Sciences at the University of Kiel, Wischhofstrasse 1-3, 24148 Kiel, Germany

ARTICLE INFO

Article history:
Received 25 November 2008
Received in revised form 14 December 2009
Accepted 1 January 2010
Available online 11 January 2010

Keywords:
Hikurangi Margin
New Zealand
hydrocarbon seeps
chemosynthesis
authigenic carbonates
mineralogy
stable isotopes
lipid biomarkers

ABSTRACT

Short box cores (to 30 cm bsf) and seafloor carbonate grab samples were acquired at mapped hydrocarbon seep sites (600–1200 m water depths) during the 2007 *RV SONNE SO191* cruise on the Hikurangi Margin offshore eastern North Island, New Zealand, to evaluate the influence of methane seepage on sedimentologic, biotic, mineralogic and stable isotopic attributes of seabed sediments. Sedimentary horizons in the box cores consist of siliciclastic silts and sands, shell beds and nodular, microcrystalline aragonite bands up to 15 cm thick. The megafauna is dominated by infaunal to semi-infaunal chemosymbiotic bivalves (*Calyptogena*, *Lucinoma*, and *Acharax*), as well as associated worms and carnivorous and grazing gastropods. Burrows in silts, some occupied by worms or juvenile *Acharax*, mainly have simple morphologies more typical of high-energy, nearshore settings than deep-sea environments, while a few are large and sparsely branched with wall scratch marks inferred to be of decapod crustacean origin.

The box core silts and nodular carbonate samples vary in TOC content from 0.2 to 0.9 wt.%, carbonate content from 4 to 78%, and $\delta^{13}C$ and $\delta^{18}O$ values from −50.3 to −0.6‰ PDB and +0.77 to +3.2‰ PDB, respectively. Low carbonate content silt samples have the most enriched $\delta^{13}C$ values, implying a seawater source for their pore water bicarbonate. Negative $\delta^{13}C$ and positive $\delta^{18}O$ values typify the nodular, microcrystalline aragonite bands, indicating formation during microbially mediated, sulphate-dependent anaerobic oxidation of methane (AOM) in a cold, near-seafloor environment, as is also supported by lipid biomarker data. A clear isotopic mixing trend of decreasing $\delta^{13}C$ and increasing $\delta^{18}O$ and carbonate content in the fine (<100 μm) carbonate fraction of the host silts also has been reported from other methane seep provinces, and suggests a heterogeneous influx of methane-rich seep fluids through the shallow seabed, displacing pore waters of seawater origin.

Seafloor grab carbonate samples show greater textural variability and are divided into two types. Fresh-appearing, grey to white blocks yield similar mineralogic, isotopic and biomarker signatures to the nodular carbonate bands in the cores. A largely seep-related epifauna affiliated with these grab samples include chemosymbiotic bathymodiolin mussels, siboglinid tube worms, methanotrophic suberitid sponges and grazing limpets which, in places, are entombed within the carbonate. By contrast, some dark reddish to brown, iron-stained, microcrystalline dolomitic slabs and tubular concretions support abundant non-seep epifaunal encrusters from the surrounding deep sea, indicative of long exposure on the seafloor. Distinct stable isotopic signatures of these exhumed dolostones ($\delta^{13}C$ c. −20‰ PDB, $\delta^{18}O$ up to +7‰ PDB) suggest derivation from an oxidised methane pool, and pore fluid freshening by gas hydrate dissociation or from mobilized burial fluids that have undergone clay mineral dehydration.

1. Introduction

The ephemeral passage of methane and other hydrocarbons through the shallow lithosphere is manifested in the geologic record *via* precipitation of authigenic carbonates (e.g. Williams and Trainor,

* Corresponding author. Tel.: +64 9 373 7599; fax: +64 9 373 7435.
E-mail address: ka.campbell@auckland.ac.nz (K.A. Campbell).
[1] Present address: ExxonMobil Exploration Company, 233 Benmar Dr., Houston, TX 77060 USA.

0025-3227/$ – see front matter © 2010 Elsevier B.V. All rights reserved.
doi:10.1016/j.margeo.2010.01.002

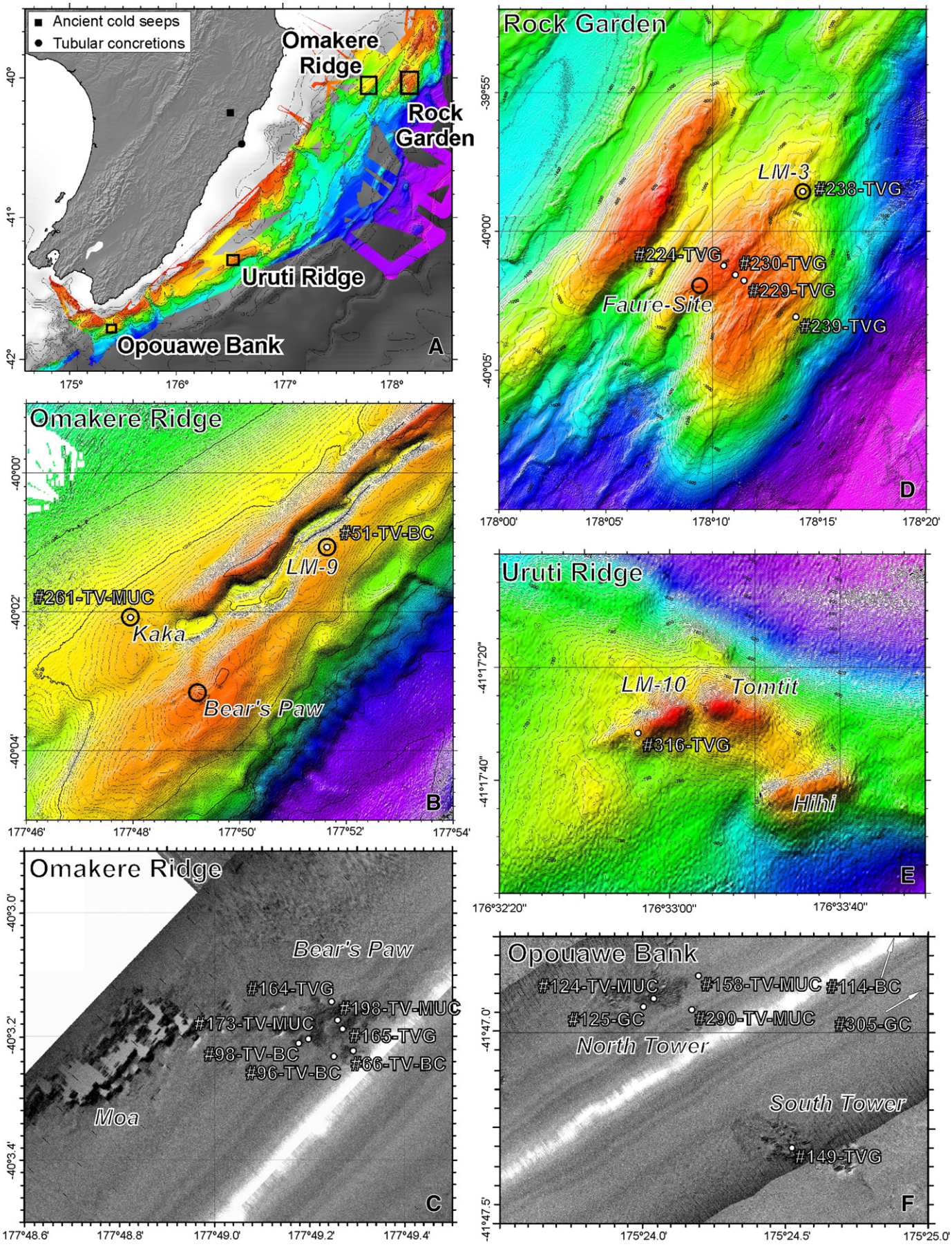
Ancient cold seeps
Tubular concretions
Omakere Ridge
Rock Garden
Uruti Ridge
Opouawe Bank
A
-40°
-41°
-42°
175°
176°
177°
178°
Rock Garden
LM-3
#238-TVG
#224-TVG
#230-TVG
#229-TVG
Faure-Site
#239-TVG
D
-39°55'
-40°00'
-40°05'
178°00'
178°05'
178°10'
178°15'
178°20'
Omakere Ridge
#51-TV-BC
LM-9
#261-TV-MUC
Kaka
Bear's Paw
B
-40°00'
-40°02'
-40°04'
177°46'
177°48'
177°50'
177°52'
177°54'
Uruti Ridge
LM-10
Tomtit
#316-TVG
Hihi
E
-41°17'20"
-41°17'40"
176°32'20"
176°33'00"
176°33'40"
Omakere Ridge
Bear's Paw
#164-TVG
#198-TV-MUC
#173-TV-MUC
#165-TVG
#98-TV-BC
#96-TV-BC
#66-TV-BC
Moa
C
-40°3.0'
-40°3.2'
-40°3.4'
177°48.6'
177°48.8'
177°49.0'
177°49.2'
177°49.4'
Opouawe Bank
#124-TV-MUC
#158-TV-MUC
#114-BC
#125-GC
#290-TV-MUC
#305-GC
North Tower
South Tower
#149-TVG
F
-41°47.0'
-41°47.5'
175°24.0'
175°24.5'
175°25.0'

Table 1
Station numbers, locations and depths, and sample label names with sample collection gear (TV, TV guided; BC, box core; MUC, multicore; GC, gravity core; G, grab).

Station and area	Seep site	Latitude (S)	Longitude (E)	Depth (m)	Gear	Sample label
Omakere Ridge						
SO191-2 #51	LM-9	40°01.076′	177°51.631′	1155	TV-BC	51-1B, -2B, -3B, -4B
SO191-2 #66	Bear's Paw	40°03.223′	177°49.293′	1097	TV-BC, TV-G	66-1A, -1B, -1C; 66-2; 66 (32) [23] B; 66 (32) [23] C; 66 (33) [16] B; 66 (45) [3] B; 66_6 [20]
SO191-2 #96	Bear's Paw	40°03.223′	177°49.256′	1096	TV-BC	96-2B
SO191-2 #98	Bear's Paw	40°03.205′	177°49.187′	1101	BC, TV-G	98-1B; 98-2B; 98 (71) [21]
SO191-2 #164	Bear's Paw	40°03.147′	177°49.239′	1080	TV-G	164 [14] B; 164 [14] D
SO191-2 #165	Bear's Paw	40°03.185′	177°49.264′	1102	TV-G	165 C; 165 [13] C; 165 [13] D; 165 [13] E
SO191-2 #173	Bear's Paw	40°03.197′	177°49.190′	1106	TV-MUC	173-B
SO191-3 #198	Bear's Paw	40°03.173′	177°49.258′	1107	TV-MUC	198
SO191-3 #261	Kaka	40°02.120′	177°47.960′	1171	TV-MUC	261
Rock Garden						
SO191-3 #224	Rock Garden	40°01.250′	178°10.470′	610	TV-G	TVG 224 Tray 1
SO191-3 #229	Rock Garden	40°01.780′	178°11.400′	660	TV-G	229 Tray 1
SO191-3 #230	Rock Garden	40°01.580′	178°11.010′	655	TV-G	230 B
SO191-3 #238	LM-3	39°58.580′	178°14.160′	907	TV-G	238 [1] TVG 17
SO191-3 #239	Rock Garden	40°03.090′	178°13.830′	891	TV-G	239 A; 239 B
Opouawe Bank						
SO191-2 #114	Tui	41°43.306′	175°27.082′	816	BC	114 (102) [15]
SO191-2 #124	North Tower	41°46.908′	175°24.024′	1051	TV-MUC	124 (123) [10]
SO191-2 #158	North Tower	41°46.850′	175°24.192′	1060	TV-MUC	158A; 158B
SO191-2 #149	South Tower	41°47.317′	175°24.487′	1053	TV-G	149 A; 149 C
SO191-2 #125	North Tower	41°46.920′	175°24.001′	1041	GC	125 (124) [11]
SO191-3 #290	North Tower	41°46.940′	175°24.200′	1059	TV-MUC	290 B
SO191-3 #305	Takahe	40°46.690′	177°25.230′	1051	GC	GC305
Uruti Ridge						
SO191-3 #316	LM-10	41°17.530′	176°32.870′	756	TV-G	316 A

1987; Mazzullo, 2000; Clari et al., 2009). At seafloor methane seeps these form as a by-product of microbially mediated, anaerobic oxidation of methane (AOM) in the sulphate reduction zone (Boetius et al., 2000). In the process, the seep-carbonates cement biotic elements of chemosynthesis-based communities, providing a window into the ecology and evolution of life in extreme environments (Sassen and MacDonald, 1998; Shapiro, 2004; Levin, 2005).

The 2007 *RV SONNE SO191* 'NEW VENTS' cruise (Greinert et al., 2010-this issue), provided a first opportunity to evaluate the textural, mineralogic, isotopic, lipidic and biotic characteristics of seep-carbonates along the convergent Hikurangi Margin, offshore eastern North Island, New Zealand (Fig. 1), first recorded by Lewis (1991) and Lewis and Marshall (1996). The seep-carbonates are modern analogues of several geographically isolated occurrences of Lower to Upper Miocene limestones exposed onshore in the uplifted forearc portion of East Coast Basin, which indicate that methane seepage has been influencing the seabed and biota offshore New Zealand since just after initiation of the current phase of subduction in the region (c. 24 Ma) (Campbell et al., 2008).

This study fingerprints the early diagenetic transformation of the initially soft, silty and sandy seabed to indurated seep-carbonate deposits, using unconsolidated box cores (0–30 cm depth bsf) collected during cruise SO191. The patterns of advecting methane seepage recorded in our core data set – comprising sedimentary textures, total organic carbon (TOC), stable carbon and oxygen isotope measurements, and carbonate and biotic contents – have the potential for excellent preservation in the geological record. We also compare the box core data with a suite of grab sample carbonates collected at seep sites during the SONNE cruise. The differences in box core *vs* grab sample analytical results highlight the complexity and heterogeneity of hydrocarbon seepage at the seafloor and in the shallow subsurface. A co-varying trend in stable isotope data is also recognized from Hikurangi Margin and other seeps elsewhere, suggesting similar biogeochemical and hydrologic processes operating in the transformation of siliciclastic seabed to indurated seep-carbonates.

2. Geotectonic setting of Hikurangi Margin seeps

The Hikurangi Margin constitutes the southernmost portion of the 3000-km-long Tonga–Kermadec–Hikurangi convergent system, where the Pacific Plate presently subducts beneath the Australian Plate (Lewis and Pettinga, 1993). Subduction began c. 24 Ma with a change from transtensional to convergent plate motion (Lewis and Pettinga, 1993; Faure et al., 2006). Plate convergence rate along the imbricated frontal wedge of the central Hikurangi subduction margin (to 150 km wide) is presently c. 43 mm/y (De Mets et al., 1990; Barnes et al., 2010-this issue). Deformation within the thick (c. 3 km) accretionary wedge of organic-rich sediments contributes to current production of a 50,000 km^2 gas hydrate province and massive methane anomalies observed offshore today (Henrys et al., 2003, 2010; Faure et al., this issue). Fluid over-pressuring is enhanced by both low-permeability mudrocks in the forearc, and containment of over-pressures in a compressional thrust-fault regime (Sibson and Rowland, 2003). An annual fluid expulsion rate of $>2\times10^6$ m^3 per 100 km along the strike-length of the margin has been estimated (Sibson and Rowland, 2003). Hydrocarbon seepage is rife along the margin today, and includes onshore and offshore fluid expulsion sites, chemosynthesis-based communities, hydrocarbon indications in industry seismic reflection

Fig. 1. Locations of core and seep-carbonate grab samples evaluated in this study, collected in 2007 from SONNE SO191, Hikurangi convergent margin, offshore eastern North Island, New Zealand. Also shown are some onshore sites of Miocene seafloor seep limestones and tubular concretions, the latter interpreted to be seep plumbing features (see Nyman et al., 2010-this issue).

data, and a prominent bottom simulating reflection (BSR) inferred as the base of the gas hydrate stability zone (see references in Campbell et al., 2008, and Barnes et al., 2010-this issue).

The five seep areas visited during cruise SO191 – Builders Pencil (Ritchie Ridge), Rock Garden, Omakere Ridge, Uruti Ridge, Opouawe Bank – all lie on the crests of thrust-faulted ridges at mid-slope depths (600–1200 m) (Greinert et al., 2010-this issue). They are positioned near the seaward edge of Cretaceous and Paleogene foundation rocks, which constitute a relatively impermeable backstop that focuses fluid migration offshore today *via* major low-angle thrust faults and the décollement (cf. Lewis and Marshall, 1996; Barnes et al., 2010-this issue). Fault fracture networks are visible in the seismic images beneath the seeps, and the BSR is disturbed at these locations by fluid and gas migration to the seafloor seep sites (Barnes et al., 2010-this issue).

3. Methods and samples

Samples were retrieved from soft-bottom sediments in methane seep areas in February and March 2007, during Legs 2 and 3 of cruise SO191, using a box corer, multicorer and gravity corer (Greinert et al., 2010-this issue). This paper focuses largely on the box core sediments. A small comparative collection of indurated seep-carbonate slabs and blocks also was obtained from the seafloor utilising a TV-guided grab sampler. For all samples evaluated herein, site location details are shown in Fig. 1 and Table 1.

Sediment cores were split and photographed on deck (e.g. Figs. 2 and 3), and live specimens collected and preserved in formalin. The refrigerated cores were logged within a few days of return from the cruise. In particular, we recorded stratigraphic position of the *in situ* megabenthos, including burrows, and delineated texturally distinct sedimentary horizons (labeled A, B, C, etc., e.g. Fig. 3). These were identified by colour and texture (e.g. reddish, greyish, brownish, and degree of grittiness), contact relationships (i.e. sharp, gradational, planar, and irregular), relative extent of carbonate induration, character and orientation of shelly infauna, and change in bioturbation pattern. The fine-grained siliciclastic sediments hosting the carbonate were sub-sampled for grain size analysis using a Malvern Mastersizer 2000 particle size analyzer. Grain size data were processed using GRADISTAT Version 4.0 software (Blott and Pye, 2001). Dominant peaks are shown as an average grain size chosen by the program, and the textural class listed for each sediment horizon follows the scheme of Folk and Ward (1957).

Several representative cut slabs (5–8 cm thick; e.g. Fig. 3) were X-rayed immediately upon arrival onshore to obtain more detailed spatial relationships amongst the siliciclastic silt/sand horizons, nodular microcrystalline carbonate bands, and infaunal biotic distributions. Sub-samples were taken from each horizon for assessment of physical and geochemical properties of the sediments (see below). Two slabs (51-1B, -2B; Fig. 3A, B) were cut (each $21 \times 28 \times 8$ cm) and analysed from one box core from station SO191/2-51 at LM9, Omakere Ridge, to examine heterogeneity of the alternating silt and nodular carbonate horizons. Another slab (98-2B) was evaluated from a box core (Fig. 2C) taken at SO191/2-98, LM9 South, which displays sharp vertical changes in carbonate content and biota. Another slab (66-1B; Fig. 3C) was studied from a box core from station SO191/2-66 at LM9, which contains a shell bed of vesicomyid bivalves and a few *in situ* *Lamellibrachia* sp. in relatively sandy sediments (Fig. 2A, B). Finally, a silt-dominated multicore (158A; 11 cm in diameter) from station SO191/2-158 at North Tower, Opouawe Bank, was chosen for analysis

Fig. 2. Entire box cores on deck displaying a *Calyptogena* shell bed (core 66) with two *in situ* tubeworms (arrows), in top view (A) and side view (B); and core 98 (C) with *Acharax* and its burrows in brown sandy silt (horizon B), overlying a nodular carbonate-cemented vesicomyid shelly accumulation (horizon A).

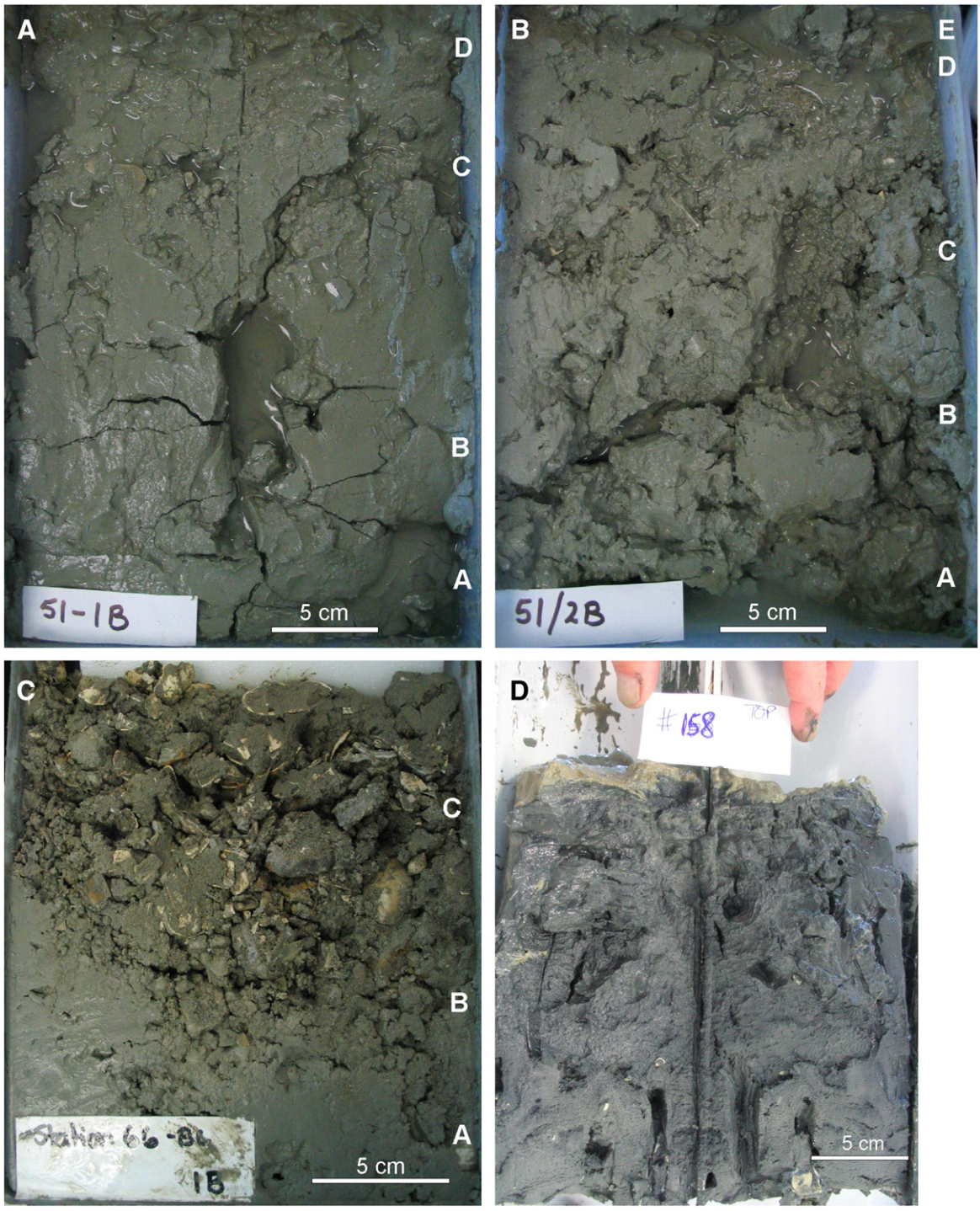

Fig. 3. Representative slabs from cores of this study showing variation in stratigraphy (horizons A, B, C, etc.) and shelly biota. (A) 51-1B box core slab; alternating horizons of sandy silt (smooth brownish grey) and nodular authigenic carbonate (irregular fabric). (B) 51-2B box core slab; sandy silt and dense, coalesced carbonate nodule development. (C) 66-1B box core slab; illuminating *Calyptogena* shell bed (horizon C) underlain by nodular authigenic carbonate (horizon B) and silty sand (horizon A). (D) 158A, split multicore; dominated by strong vertical, branching bioturbation fabric.

as it reveals a strong and distinctive bioturbated fabric (Fig. 3D). Additional box core and multicore descriptive data can be found in Boyd (2009).

X-ray diffraction (XRD) analysis (Philips PW1130 generator and PW1050/25 goniometer) was used to determine the mineralogy of samples. After powdering, carbonate samples were run from 20 to 40°2θ, and stepped at 0.02° at a speed of 0.5°/min, with operating conditions of 40 kV and 20 mA. Semi-quantitative estimates of mineral abundances were made based on relative peak heights within and between sample runs, using the procedure of Nelson and Cochrane (1970). Clay mineral determinations were made using wet sub-samples centrifuged with hexametaphosphate that were dried onto glass slides. They were run, both air dried and glycolated, at 2 to 20°2θ, with a step size of 0.02° and a speed of 3°/min.

Total organic carbon (TOC) and carbonate content were measured for selected box core siliciclastic horizons, and for box core and grab

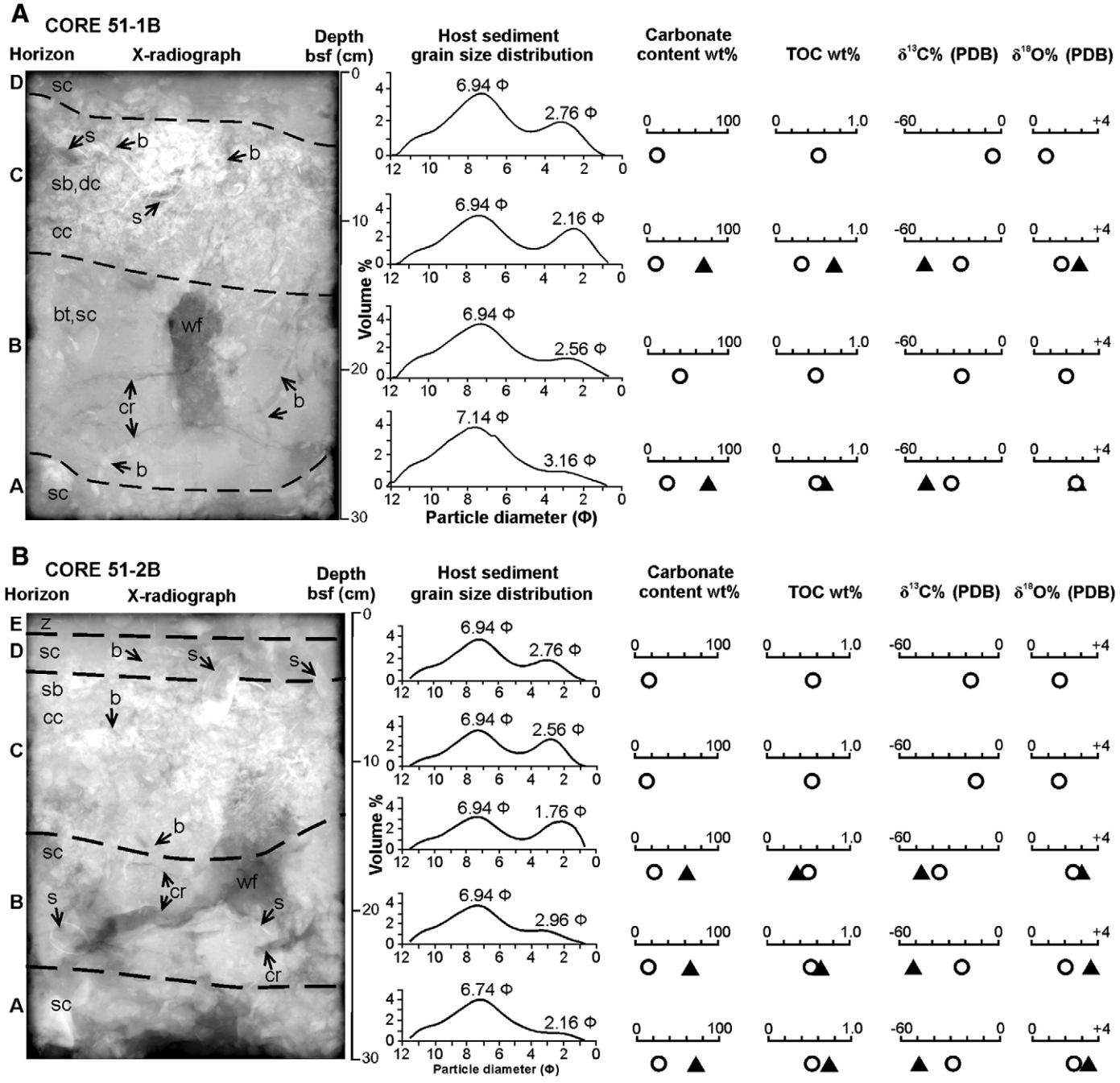

Fig. 4. Two representative box core 51 slabs – (A) 51-1B and (B) 51-2B – with alternating sandy silt and nodular carbonate horizons, cut vertically in sequence to illuminate small-scale spatial changes in seafloor siliciclastic sediments influenced by methane seepage and authigenic carbonate formation. X-radiograph, grain size distributions, carbonate content, TOC (total organic carbon), and carbon and oxygen isotope results, by horizon, are shown. Symbols include: z, silt; bt, bioturbated silt; sc, scattered small carbonate nodules; cc, moderately dense clotted carbonate; dc, dense indurated carbonate of merged nodules; s, shell (articulated *Calyptogena* or *Lucinoma* in life position); sb, shell bed; sh, shell hash; b, burrow; wf, water feature; cr, crack; open circles, bulk fine-fraction carbonate isotope measurement from unconsolidated silt horizon; black triangles, nodular/banded authigenic carbonate isotope measurement.

carbonate samples using powdered splits, while lipid biomarkers were analysed from 18 grab samples. Total carbon (TC) content was measured in a Carlo Erba NA 1500 elemental analyzer at IFM-GEOMAR (Kiel, Germany) following combustion to CO_2 of 10–20 mg of powdered sample at 1050 °C in a tin cup. TOC was determined using the same instrument after removing carbonate carbon by acidification with 0.25 N hydrochloric acid. Samples were run in duplicate, along with an internal standard. Carbonate contents were derived from the TC minus TOC values using an internally prepared calibration curve ($y = 9.2477x - 2.8863$ where x = TC wt.%; $r^2 = 0.99$). The lipid analyses were undertaken at Geoscience Australia using the extraction and GC–MS procedures detailed by Grosjean and Logan (2007).

Stable carbon and oxygen isotope analysis was undertaken on the fine carbonate component of the core silts/sands, and on the indurated carbonates of the box core and grab samples. Samples were reacted in 105% orthophosphoric acid at 70 °C for 10 min (2 h for 3 dolomite samples) and the evolved CO_2 introduced into a Europa 20/20 mass spectrometer (University of Waikato). The isotope values are reported

in delta (δ) notation per mille (‰) deviation of the $^{18}O/^{16}O$ or $^{13}C/^{12}C$ ratio of the sample relative to the VPDB standard by repeated analyses of international standard NBS-19 and internal standard WCS. Instrument precision is ±0.05‰ for both $\delta^{18}O$ and $\delta^{13}C$, and analytical precision is ±0.05 to 0.1.

4. Results

4.1. Box core lithologies and biota

The background siliciclastic sediment in the box cores is predominantly poorly sorted sandy silt. Grain size frequency histograms for the siliciclastics of some representative box core slabs are illustrated in Figs. 4 and 5 alongside X-radiograph, TOC, carbonate content and stable isotope data for each textural horizon.

The box core carbonate horizons consist of microcrystalline carbonate (micarb) cementing siliciclastic silt and sand. The degree of development of the micarb horizons ranges from scattered nodules to dense, coalesced nodular bands up to 15 cm thick. In the X-radiograph images (Figs. 4 and 5) the carbonate-rich horizons stand out in white; whereas, grey shades constitute siliciclastic silt horizons, burrows and cracks formed during sampling (cf. Levin, 2005, her Fig. 2).

Mega-invertebrates in the box cores have a moderately low diversity but, in places, a relatively high abundance including molluscs, worms and, based on burrow features, decapod crustaceans, most of which are seep-related and some of which are derived from the surrounding deep-

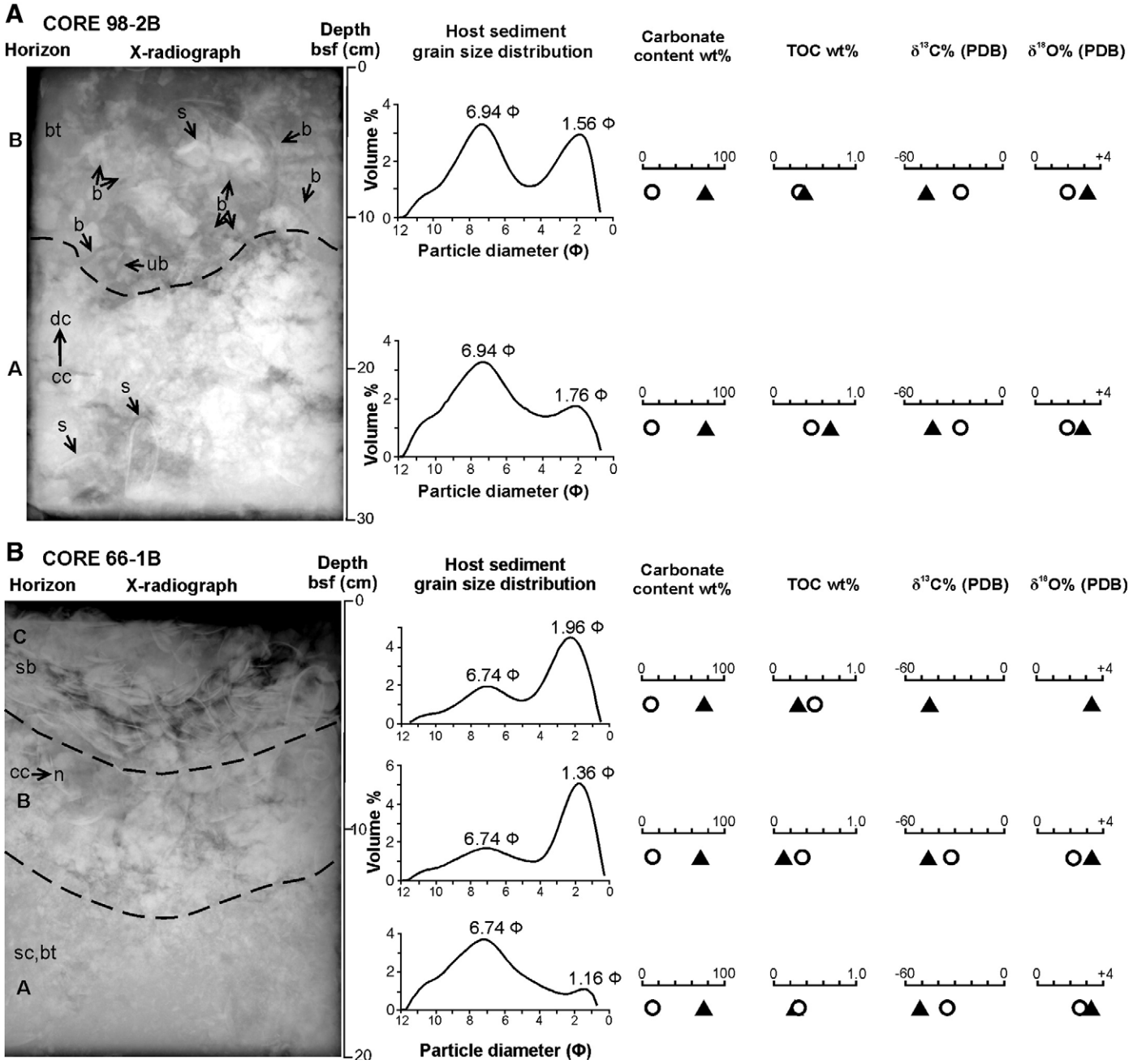

Fig. 5. Other box core textures, showing inferred transition to waning flow (A), and nodular carbonates beneath vesicomyid shell bed (B). (A) Slab 98-2B of box core 98, with upper sandy silt (horizon B) riddled with juvenile *Acharax* and its burrows, and lower nodular carbonate (horizon A) with *Calyptogena* shells. (B) Slab 66-1B of box core 66, showing a *Calyptogena* shell bed at seafloor (horizon C) underlain by nodular dense carbonate (horizon B) and silty sand (horizon A). Symbols defined in Fig. 4, except for ub, a u-shaped burrow (*Solemyatuba*) and a typical dwelling structure of solemyid bivalves; and n, a nodular horizon.

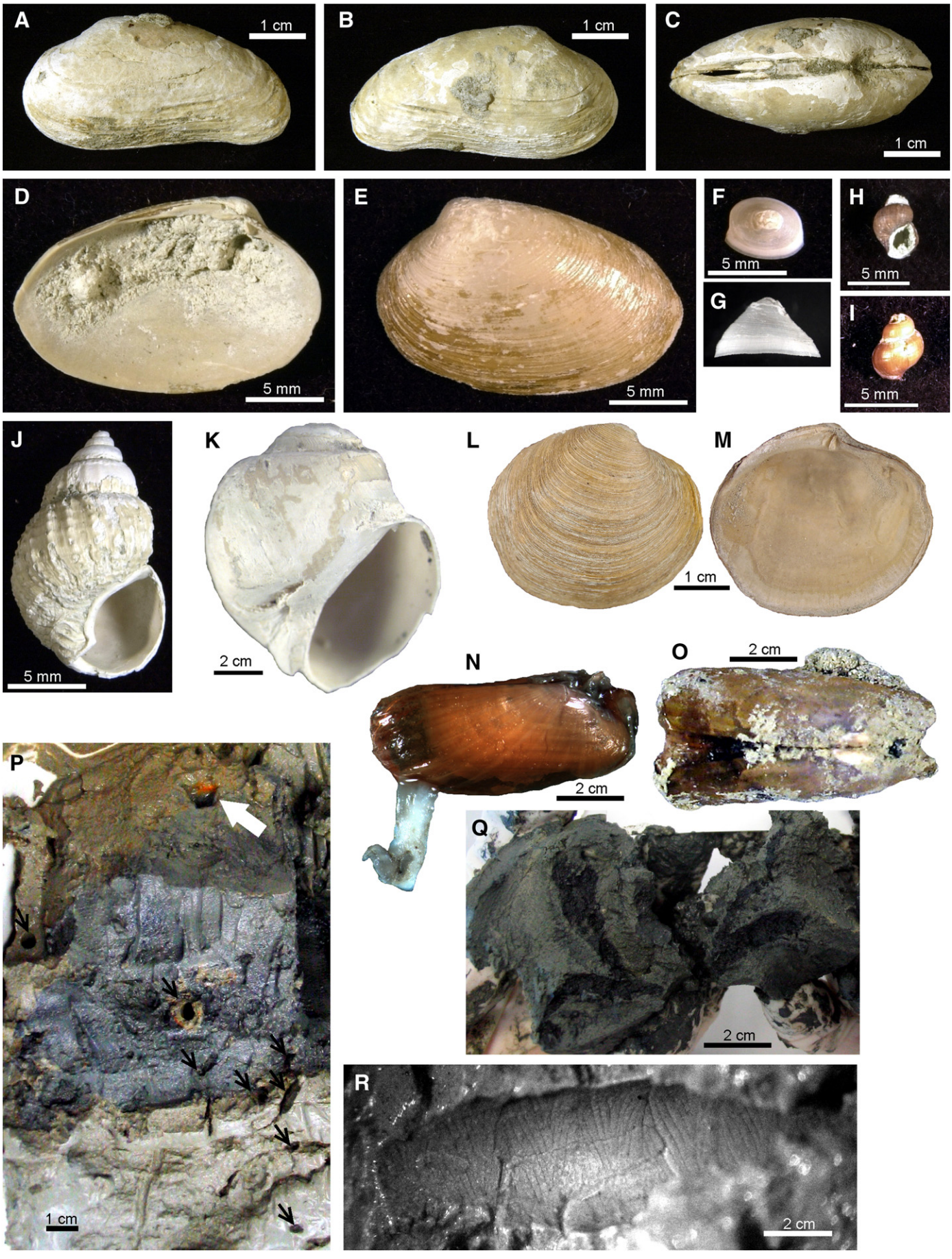
A
1 cm
B
1 cm
C
1 cm
D
5 mm
E
5 mm
F
5 mm
G
H
5 mm
I
5 mm
J
5 mm
K
2 cm
L
1 cm
M
N
2 cm
O
2 cm
P
1 cm
Q
2 cm
R
2 cm

sea environment (Fig. 6). The soft-bottom shelly taxa are mostly shallow infaunal, and chemosymbiotic or carnivorous in life habit. A few are epifaunal grazers. They include (e.g. Fig. 6A–O) the chemosymbiotic bivalves *Calyptogena* sp., *Lucinoma galathea* and *Acharax clarificata*, various gastropods such as *Nassarius ephamillus*, *Falsilunatia* sp., *Provanna* sp. and *Acteon* sp., and an unidentified limpet. Taphonomy of the shells ranges from broken to complete, and from unworn to showing signs of abrasion and dissolution. Live burrow occupants include juvenile *A. clarificata*, a terebellid worm with oxidised haloes around the 10 mm-diameter burrow opening (Fig. 6P), a sea anemone, and unidentified, thin red, white or black worms.

Several burrow types occur in the box core slabs and are imaged in the X-radiographs (Figs. 4 and 5). Morphologies range from thin (1–4 mm diameter), unlined or lined, curved vertical or undulating horizontal traces, to thicker (6 mm), sparsely branching vertical burrows with wall scratch marks (Fig. 6Q, R). Collectively they are largely representative of dwelling and movement traces. In box core 98-2B (Figs. 2C, 5A), carbonate-cemented vesicomyid bivalves (horizon A) are overlain by siliciclastic silt (horizon B) riddled with two forms of juvenile *Acharax* burrows: rare, u-shaped dwelling tubes (*Solemyatuba curvatus* of Seilacher, 1990), and abundant mobile repichnia that are unbranched, and vertically or horizontally oriented.

4.2. Grab sample lithologies and biota

Two broad categories of carbonate rock types occur in our grab sample collection, namely 'fresh' and 'weathered-looking' specimens (Fig. 7). The fresh samples are light or medium grey to whitish in colour and display variable fabrics, yielding four main textural sub-types: (1) light grey, sandy micarbs with an abundant attached or embedded shelly biota (Fig. 7A–D, H–J); (2) grey tubular (up to 2 cm diameter) micarbs with no fossils that may include open or partially sediment-filled central conduits (Fig. 7E, F); (3) porous, white to translucent, fibrous layers cementing biota (Fig. 7K); and (4) breccias of grey micarb intraclasts cemented with white fibrous cement (Fig. 7L). Many of these texturally varied, fresh carbonates contain a fine-grained siliciclastic component (Table 3). By contrast, the weathered grab samples are micarbs supporting an outer rind (1–2 mm thick) of dark reddish to brown Fe–Mn staining (e.g. Fig. 7M–O). Overall, the grab sample collection reveals more varied carbonate fabrics than occurs in the monolithic, clotted to densely nodular micarb horizons of the box cores (e.g. Fig. 3A–C).

The taphonomic state of the organisms and shells associated with (i.e. incorporated within or attached to) the grab sample carbonates ranges from pristine (some live) to worn, broken, leached and/or iron-stained (e.g. Fig. 7). The fresh-looking, lighter coloured carbonates typically entomb or are encrusted with abundant and diverse biotic remains, including heterotrophs (e.g. naticid gastropods, spicules of unidentified siliceous sponges; Fig. 7A, B), and seep-related taxa, such as siboglinid tubeworms, limpets, suberitid sponges, and vesicomyid or bathymodiolin bivalve shell beds/hashes (cf. Thurber et al., 2010-this issue; e.g. Fig. 7C, D, G–K). *Calyptogena* dominated, sand-rich carbonate blocks and shell hashes (e.g. Figs. 2B, 3C, 7I) are spatially distinct from mussel-dominated occurrences in Hikurangi Margin micarb blocks (e.g. Fig. 7H, J). Some indurated bathymodiolin shell hashes support live mussel, tubeworm and methanotrophic sponge-commensal communities (e.g. Fig. 7G, H, J, station 238, LM-3, Rock Garden; cf. Thurber et al., 2010-this issue). In a number of cases, old open burrows or fluid conduits are now utilised by living tubeworms (e.g. Fig. 7C). In other samples, cemented tubular moulds (Fig. 7K) impart a strong biogenic fabric to the rock, with the moulds displaying the same range in diameters as living siboglinid tubeworms brought to the surface in the grab hauls.

In comparison, the strongly Fe/Mn-stained, weathered carbonates have been heavily bored and encrusted with a diverse and abundant epifauna typical of deep-sea hardgrounds (e.g. Fig. 7M–O), including hydroids, bryozoans, octocoral, stony coral, stylasterids, serpulid worms and calcareous sponges. No typical seep-related taxa are evident within or upon these iron-stained micarb grab samples.

4.3. Mineralogy, TOC and carbonate content

The mineralogy, TOC and carbonate content of the box core siliciclastic silts/sands and the box core and grab carbonates are summarised in Tables 2 and 3 and in Fig. 8. Core silts and sands range in fine-fraction (<100 μm) carbonate content (i.e. excluding any whole shells) from 4 to 27 wt.%. TOC values are highest (0.74–0.92 wt.%) in sand-free silts and lowest (0.24–0.57 wt.%) in sandy silts, with the lowest value extracted from the sandiest sample (66-1B, horizon A). Box core micarb nodules and bands have moderately high carbonate contents (63–77 wt.%) (Table 2) and a broad range of TOC values (0.1–0.9 wt.%), similar to results for the grab sample carbonates (Fig. 8, Table 3). However, distinct mineralogic differences exist in the sample data set. Aragonite is the dominant mineralogy of the box core micarb bands and the fresh carbonate grab samples, irrespective of their fabrics. Minor amounts of high-Mg calcite (HMC) occur in several nodular core carbonate bands (Tables 2 and 3). Quartz and plagioclase feldspar are minor components of many of the box core and grab carbonate samples (Tables 2 and 3). The unconsolidated box core silts/sands are quartz and plagioclase rich, and typically also include a significant clay mineral component dominated by smectite and illite with common kaolinite. Their carbonate mineral content is usually minor, composed mainly of low-Mg calcite (LMC), and some HMC and aragonite (Table 2). By contrast, the Fe/Mn-stained carbonate slabs and blocks encountered in grab samples are composed of microcrystalline dolomite. They also have extremely low TOC values (Fig. 8).

4.4. Stable isotopes

Stable carbon and oxygen isotope measurements from the box core nodular/banded carbonate, the grab carbonate, and the bulk fine-fraction carbonate within the unconsolidated box core sediments are shown in Tables 2 and 3. A $\delta^{13}C$ *vs* $\delta^{18}O$ cross-plot of these data (Fig. 9A) reveals a linear trend of decreasing $\delta^{13}C$ with increasing $\delta^{18}O$, from end-member silts with $\delta^{13}C$ and $\delta^{18}O$ values near 0‰ PDB, to tightly clustered values for the microcrystalline aragonite nodules and blocks in the vicinity of $\delta^{13}C$ −50‰ PDB and $\delta^{18}O$ +3‰ PDB. By contrast, the Fe/Mn-stained dolomitic micarb slabs yield more enriched $\delta^{18}O$ values (+6.4 to +6.9‰ PDB) and moderately depleted $\delta^{13}C$ values (c. −20‰ PDB), forming a separate and distinctive isotopic field (Fig. 9A).

The linear trend displayed in the authigenic carbonate isotope data is analysed further in Fig. 10, a 3D box plot of carbonate content *vs* carbon

Fig. 6. Representative biota and taphonomy, from selected box cores. (A–C) Worn and carbonate-cemented vesicomyid bivalve, *Calyptogena* sp., articulated individual. Box core 51-2B (Fig. 4B) at contact between horizons C and D. (D, E) Inner and outer shell of vesicomyid bivalve with partially carbonate-cemented interior. Box core 51-2B, horizon C. (F, G) Patelliform gastropod, apical and side views. Box core 51-2B, horizon C. (H) Provannid gastropod, apertural view. Multicore, station 186. (I) Provannid gastropod, abapertural view. Box core 51-2B, horizon A. (J) Carnivorous gastropod, *Nassarius ephamillus*. Box core 51-2B, horizon B. (K) Predatory naticid gastropod, *Falsilunatia* sp., apertural view. Box core 51-2B, horizon C. (L, M) Lucinid bivalve, *Lucinoma galathea*, right and left valves, respectively. Box core 51-1B (Fig. 4A), horizon C. (N) Live juvenile solemyid bivalve, *Acharax clarificata*, with white fleshy foot emergent from the anterior portion of the valves. Multicore 242, horizon B, 6 cm bsf. (O) Worn and carbonate-cemented juvenile solemyid bivalve, *Acharax clarificata*, with splayed valves. Box core 98-1B. (P) Top of box core 158A, partially cut-away view (where dark grey in colour), showing several circular, horizontal to obliquely vertical burrow openings (black arrows), with red tentacles of a terebellid worm (white arrow) emergent through upper opening. Where burrow cross-sections are exposed at depth in grey (reducing) sediments they display lighter-coloured, oxidised sediment haloes about their walls (e.g. central portion of photo). (Q) Branched vertical burrows in lower part of box core 158A, with dark, sulphide-rich coatings on burrow walls. (R) Burrow detail (*Spongeliomorpha* isp.) from vertically branching burrows at base of 158A, showing wall scratch marks, indicative of decapod crustacean activities.


A
1 cm
B
1 cm
C
1 cm
D
5 mm
E
F
1 cm
G
5 mm
H
I
1 cm
J
1 cm
K
1 cm
L
1 cm
M
1 cm
N
1 cm
O
1 cm

and oxygen isotope values for only the core fine-fraction carbonates. Decreasing $\delta^{13}C$ is accompanied by an increase in carbonate content (range 4–27 wt.%) and enrichment in $\delta^{18}O$. The data points exhibit a narrow spread along the linear trend for those samples with $\delta^{13}C$ values > −20‰ PDB, which consist of low carbonate siliciclastic silts. In the more ^{13}C-depleted samples ($\delta^{13}C$ −20 to −38‰ PDB), typified by coarser sandy silts and silty sands, the fine-fraction carbonate data points become more widely dispersed.

4.5. Lipid biomarkers

The biomarker types in the 16 analysed aragonitic grab samples fall into one of three groups (Fig. 11). The first shows relatively simple lipid distributions with high abundances of archaeol, hydroxyarchaeol, crocetane and the irregular isoprenoid 2,6,10,15,19-pentamethylicosane (PMI). Hydroxyarchaeol typically dominates the biomarker distributions. The illustrated example (Fig. 11A) shows the highest concentrations of crocetane, PMI, archaeol and *sn*-2 hydroxyarcheol (hydroxylated at C-3 in the *sn*-2 phytanyl moiety), respectively 1.2, 0.2, 2.4 and 4.5 μg/g of dry sediment. *sn*-3 hydroxyarchaeol (hydroxylated at C-3 in the *sn*-3 phytanyl moiety) is detected in very low abundances as a shoulder of the *sn*-2 hydroarchaeol peak (Fig. 11A). Also present in this first group of samples are a series of mono-unsaturated crocetenes and unsaturated PMIs (1 to 4 double bonds), phytanol and non-isoprenoidal dialkyl glycerol diethers (DGDs) (Fig. 11A). The second group of samples has the same biomarkers as the first, but in addition includes various algal compounds such as long-chain alkenones, alkyl diols and sterols (Fig. 11B) (Volkman et al., 1998). Terrestrial lipids also are represented by C_{26}–C_{32} *n*-alkanols and *n*-alkanoic acids showing a strong even over odd carbon number predominance (Volkman, 1986). A third group of samples is characterised by only low abundances of crocetane, PMI, archaeol and hydroxyarcheol, with the two last biomarkers listed being, on average, ~10 and ~30 times lower in concentrations, respectively, than in aragonite dominated grabs from the two other groups.

In contrast to the above aragonite dominated samples, the two analysed Fe/Mn-stained dolomitic grab samples entirely lack crocetane, PMI, archaeol and hydroxyarcheol, and instead are composed of sterols and fatty acids with cholesterol as the dominant component (Fig. 11C).

5. Discussion

5.1. Evidence for AOM and MDACs on the Hikurangi Margin

Methane derived authigenic carbonates (MDACs) form as a by-product of microbially mediated, anaerobic oxidation of methane (AOM) in the sulphate reduction zone (SRZ) at or just beneath the seafloor (e.g. Irwin et al., 1977; Boetius et al., 2000; Judd and Hovland, 2007). Results indicate the main carbonate component in Hikurangi Margin *in situ* box cores and associated seafloor grab samples is MDAC, as supported by the following properties:

(a) A mineralogy overwhelmingly dominated by microcrystalline aragonite, along with a wide range of massive to crustose to occasionally laminated fabrics that are typical of those derived from microbially mediated AOM in near-seafloor SRZ at sites of active methane venting and/or shallow subsurface gas hydrate dissociation (e.g. Roberts and Aharon, 1994; Bohrmann et al., 1998; Naehr et al., 2000, 2007; Aloisi et al., 2000, 2002; Greinert et al., 2001; Peckmann et al., 2001; Teichert et al., 2005a, b).

(b) A rather tight cluster of strongly negative $\delta^{13}C$ values in the vicinity of −50‰ PDB for both the box core micarb nodules/bands and most of the grab samples, indicating the importance of AOM during carbonate precipitation (Campbell, 2006, and references therein).

(c) High abundances of crocetane, PMI, archaeol and hydroxyarchaeol lipids in the analysed aragonitic grab samples that are typical of those in carbonates forming at active methane seeps, and which have been assigned to methanotrophic archaea involved in AOM (Pancost et al., 2001; Thiel et al., 2001; Hinrichs and Boetius, 2002). The dominance of hydroxyarchaeol over archaeol, the prevalence of the *sn*2-hydroxyarchaeol isomer over *sn*-3 and the presence of crocetane have been suggested to be diagnostic for anaerobic methanotrophic archaea of the phylogenetically distinct group ANME-2 (Blumenberg et al., 2004; Pancost et al., 2005). The presence of non-isoprenoidal DGDs from sulphate-reducing bacteria constitutes supporting evidence for sulphate-dependent AOM processes.

(d) A strong spatial association of chemosymbiotic taxa (*Calyptogena*, *Lucinoma*, *Acharax*) reliant on by-products of AOM, such as the presence of sulphides in seep sediments (cf. Ritger et al., 1987; Sahling et al., 2002).

5.2. Fluid sources and migration reflected in stable isotopes of MDACs

5.2.1. Carbon sources of Hikurangi Margin MDACs

The linear trend displayed in the carbon isotopes of Hikurangi Margin box core carbonates (Fig. 9A) appears to mirror the full spectrum of pore water mixing amongst potential carbon sources — from oxidised biogenic methane and/or thermogenic methane to seawater bicarbonate. Samples with $\delta^{13}C$ values nearer to 0‰ PDB come from the relatively low background carbonate in the box core siliciclastic silts/sands (Figs. 8, 9A, 10), reflecting ambient seafloor, non-seep pore fluids. The most depleted $\delta^{13}C$ values nearer to −50‰ PDB were sampled exclusively from aragonitic micarb nodules within the box cores and fresh grab samples (i.e. high carbonate samples) that formed within active seepage areas. Along the Hikurangi Margin, natural hydrocarbon seeps and pore fluids from oil and gas wells at both onshore and offshore sites indicate a range of fluid origins, from entirely biogenic methane to entirely thermogenic methane to mixed sources (Lyon et al., 1992a,b; Francis, 1998; Lowry et al., 1998; Davies et al., 2000; Tap Oil Ltd, 2004). Based on other studies elsewhere, we infer a sufficient supply of shallow and/or deep methane to Hikurangi Margin seeps that would adequately account for the range in $\delta^{13}C$ values of the carbonates. However, based on the stable isotope data alone, we cannot rule out input from other carbon sources such as marine bicarbonate and organic matter degradation (cf. Joye et al., 2004; Peckmann et al., 2009).

Fig. 7. Representative biota and taphonomy, from seafloor carbonates that were collected with a TV-guided grab sampler. (A) Naticid gastropod, *Falsilunatia* sp., situated upon authigenic microcrystalline aragonite that cemented around siliceous sponge spicules. SO191-2 51 (8) [9] B. (B) Glass sponges incorporated into micarb aragonite. SO191-2 51 (8) [9] A. (C) Indurated micarb aragonite with live-collected tubeworm (white arrows, now dried) occupying previously formed burrow or fluid conduit opening. SO191-2 66 45 3 B. (D) Patelliform gastropods (arrows) nestling amongst cracks and irregular topography of indurated micarb aragonite. SO191-2 238 1. (E, F) Tubular microcrystalline carbonate concretion with central hole partially filled by lighter coloured sediment. SO191-2 124 123 10. (G) Detail of siboglinid tubeworm encrusted with live suberitid sponge, both chemosymbiotic. SO191-2 238 TVG-17. (H) Shipboard haul of epifauna associated with aragonite-cemented mussel-shell hash, including live siboglinid tubeworms, suberitid sponges and bathymodiolin mussels (arrows). SO191-2 238 TVG-17. (I) Disarticulated, broken *Calyptogena* shells cemented into micarb aragonite. SO191-2 165 13 C. (J) Detail of micarb aragonite-cemented mussel-shell hash of (H). SO191-2 238 TVG-17. (K) Layers of opaque white to translucent aragonite with high primary porosity, including cemented moulds of tubeworms (arrows). SO191-2 138 (181) [12]. (L) Poorly sorted breccia of subrounded grey micarb intraclasts cemented with white aragonite layers. SO191-3 316 A. This fabric is closely similar to Hydrate Ridge breccias from a seafloor chemoherm (Teichert et al., 2005a, their Fig. 5F), and aragonite crusts associated with gas hydrates (Greinert et al., 2001, Plate I, sample McB-ap). (M) Collection of small dolomitic micarb tubes with open central conduits, stained with a brown Fe/Mn coating, bored, and encrusted with coral, serpulid worm tubes and bryozoa. SO191-3 224. (N) Dolomitic micarb block, stained with a brown Fe/Mn coating, bored, and encrusted with coral, hydroids and bryozoa. SO191-3 224. (O) Cut slab of dolomitic micarb block, illuminating outer red-brown weathering rind of iron oxides and surface borings. SO191-3 239 B.

Table 2
Analytical results for core samples of nodular/banded carbonate and siliciclastic horizons (Horiz.) in this study. TOC, total organic carbon. Mineralogy (minor minerals italicised in brackets): Qtz, quartz; Plag, plagioclase feldspar; K-feld, K-feldspar; Arag, aragonite; LMC, low-Mg calcite; HMC, high-Mg calcite. Clay minerals (not shown), in siliciclastic samples, were mainly smectite and illite, with some kaolinite.

Lab no.	Core no.	Horiz.	Lithology	Carbonate wt.%	TOC wt.%	δ^{13}C ‰ PDB	δ^{18}O ‰ PDB	Mineralogy *(Minor)*
C29	51-1B	D	Siliciclastic	10.8	0.566	-5.47	0.77	Qtz *(Plag, LMC)*
C73	51-1B	C	Carbonate	64.7	0.659	-47.80	2.92	Arag *(Qtz)*
C30	51-1B	C	Siliciclastic	17.6	0.355	-23.57	1.71	Qtz *(Plag, LMC, Arag)*
C31	51-1B	B	Siliciclastic	20.2	0.500	-24.8	2.02	
C32	51-1B	A	Siliciclastic	23.8	0.497	-30.77	2.32	
C72	51-1B	A	Carbonate	75.4	0.597	-46.68	2.70	Arag *(LMC, HMC, Qtz)*
C33	51-2B	E	Siliciclastic	13.5	0.545	-16.92	1.54	
C34	51-2B	D	Siliciclastic	11.7	0.517	-14.01	1.39	
C76	51-2B	C	Carbonate	62.5	0.358	-49.14	2.94	Arag, Qtz *(LMC, HMC)*
C35	51-2B	C	Siliciclastic	19.8	0.452	-34.98	2.48	Qtz, Plag, Arag *(LMC, HMC)*
C75	51-2B	B	Carbonate	67.0	0.646	-50.29	3.21	Arag *(Qtz)*
C36	51-2B	B	Siliciclastic	17.6	0.491	-22.03	1.96	Qtz *(Plag, LMC, HMC)*
C74	51-2B	A	Carbonate	72.4	0.743	-49.14	3.14	Arag *(Qtz)*
C37	51-2B	A	Siliciclastic	23.8	0.469	-29.67	2.43	Qtz *(Plag, L/HMC, Arag)*
C38	51-3B	C	Siliciclastic	10.7	0.550	-9.37	1.15	Qtz, Plag *(LMC)*
C78	51-3B	B	Carbonate	64.6	0.274	-48.43	2.99	Arag *(LMC, Qtz, Plag)*
C39	51-3B	B	Siliciclastic	27.1	0.406	-37.70	2.61	Qtz *(Plag, Arag, L/HMC)*
C77	51-3B	A	Carbonate	62.2	0.311	-47.78	3.01	Arag *(LMC, HMC, Qtz)*
C40	51-3B	A	Siliciclastic	18.9	0.456	-22.55	1.97	Qtz *(Plag, LMC, HMC)*
C42	51-4B	C	Siliciclastic	19.1	0.443	-29.34	2.17	Qtz, Plag *(LMC, Arag, HMC, K-feld)*
C43	51-4B	C	Siliciclastic	20.8	0.504	-27.74	2.24	Qtz *(Plag, L/HMC, Arag)*
C80	51-4B	B	Carbonate	70.2	0.580	-49.34	3.05	Arag *(LMC, Qtz)*
C44	51-4B	B	Siliciclastic	17.7	0.566	-20.49	1.85	Qtz *(Plag, LMC, HMC)*
C79	51-4B	A	Carbonate	78.0	0.330	-49.96	3.20	Arag, Qtz *(Plag)*
C45	51-4B	A	Siliciclastic	18.3	0.489	-24.52	1.99	Qtz, Plag, LMC *(HMC)*
C82	98-2B	B	Carbonate	67.7	0.286	-48.73	3.03	Arag *(Qtz)*
C57	98-2B	B	Siliciclastic	13.7	0.344	-24.49	1.90	Qtz *(Plag, Arag, LMC)*
C81	98-2B	A	Carbonate	76.6	0.701	-49.27	3.12	Arag *(Qtz)*
C58	98-2B	A	Siliciclastic	14.6	0.420	-29.53	2.42	Qtz *(Plag, Arag, L/HMC)*
C85	66-1B	C	Carbonate	67.7	0.288	-48.28	3.08	Arag *(Qtz, Plag)*
C46	66-1B	C	Siliciclastic	4.6	0.460			Qtz *(Plag, LMC)*
C47	66-1B	B	Siliciclastic	33.6	0.419	-44.39	2.92	Qtz, Plag, Arag *(LMC, HMC)*
C84	66-1B	B	Carbonate	71.2	0.115	-49.16	3.17	Arag, Qtz *(Plag)*
C48	66-1B	B	Siliciclastic	10.1	0.329	-36.56	2.22	Qtz, Plag *(Arag, LMC)*
C83	66-1B	A	Carbonate	75.4	0.253	-50.30	3.10	Arag *(Qtz)*
C49	66-1B	A	Siliciclastic	14.1	0.457	-28.78	2.02	
C50	66-1B	A	Siliciclastic	10.8	0.236	-36.48	2.61	Plag *(Qtz, Arag)*
C59	158A	B	Siliciclastic	4.1	0.923			Qtz *(Plag, LMC, HMC)*
C60	158A	A	Siliciclastic	5.0	0.830	-0.63	0.99	Qtz, Plag *(LMC)*
C51	96-2B	C	Siliciclastic	8.9	0.450	-0.28	0.69	Qtz *(Plag, LMC, HMC)*
C52	96-2B	B	Siliciclastic	8.9	0.412	-0.17	0.43	Qtz, LMC *(Plag)*
C53	96-2B	A	Siliciclastic	10.6	0.447	-0.11	0.54	Qtz, LMC *(Plag)*
C54	98-1B	C	Siliciclastic	13.5	0.337	-25.32	1.88	Plag *(Qtz, LMC, Arag)*
C55	98-1B	B	Siliciclastic	17.3	0.360	-34.52	2.23	Qtz *(Plag, Arag, LMC)*
C56	98-1B	A	Siliciclastic	14.3	0.398	-26.40	2.00	Qtz *(Plag, LMC, Arag, HMC)*
C61	173-B	B	Siliciclastic	9.7	0.481	-6.88	0.91	Qtz *(Plag, LMC)*
C62	173-B	A	Siliciclastic	13.6	0.362	-14.10	1.58	Plag, Qtz *(LMC)*
C63	261	C	Siliciclastic	0.8	0.479	-0.52	1.44	
C64	261	B	Siliciclastic	10.2	0.338	-26.97	2.66	
C65	261	A	Siliciclastic	6.9	0.548	-2.18	0.04	Qtz, Plag *(LMC, K-feld)*
C66	305-D	D	Siliciclastic	6.0	0.788	1.50	0.88	Qtz *(Plag, LMC, HMC)*
C67	305-C	C	Siliciclastic	6.1	0.742	1.51	0.89	Qtz *(Plag, LMC, HMC)*
C68	305-B	B	Siliciclastic	6.2	0.791	1.19	0.94	Qtz, Plag *(LMC, HMC)*
C69	305-B	B	Siliciclastic	5.9	0.765	1.49	0.84	Qtz *(Plag, LMC)*
C70	305-B	B	Siliciclastic	8.0	0.777	1.38	0.73	Qtz, Plag *(LMC, HMC)*
C71	305-A	A	Siliciclastic	6.1	0.748	1.38	0.83	Qtz *(Plag, LMC, HMC)*

In general, carbon isotope signals of pore water bicarbonate at seeps reveal the degree to which the methane-C reservoir is oxidised (Claypool and Kaplan, 1974; Whiticar, 1999), and the amount of mixing with other carbon sources (e.g. oxidised organic matter, microbial fermentation, thermogenic methane, seawater, etc.; Suess and Whiticar, 1989; Aharon, 2000). These pore fluid attributes are manifest at seep provinces within texturally, mineralogically and geochemically varied carbonates, such as at Monterey Bay (Stakes et al., 1999), Hydrate Ridge (e.g. Kulm and Suess, 1990; Greinert et al., 2001) and in samples from the Hikurangi Margin. Whether the heterogeneous carbonates from these locales are simply more intensively sampled and better studied than in other regions, or whether some seep provinces naturally develop a greater number of carbonate lithotypes with more biogeochemical variety, is unknown at present. Biogeochemical variability may be related to uplift and exhumation intensity and duration, leading to sampling of a greater cross-section of diagenetic environments of the sediment column, with fluid flow and material transport driven by active faulting, diapirism, tectonic erosion, or other processes (cf. Greene et al., 1999; Orange et al., 1999).

5.2.2. Oxygen sources of Hikurangi Margin MDACs

Oxygen isotope values of authigenic carbonates can illuminate the composition and temperature of pore fluids at the time of carbonate precipitation (Longstaffe, 1987). Using an estimated range of −0.5 to

Table 3
Analytical results for grab sample carbonates and cemented siliciclastics. Abbreviations defined in Table 2.

Lab no.	Sonne label	Carbonate wt.%	TOC wt.%	$\delta^{13}C$ ‰ PDB	$\delta^{18}O$ ‰ PDB	Mineralogy *(Minor)*
C86	SO191-27 [18] A			-49.45	3.21	Aragonite
C87	SO191-27 [18] B			-51.23	3.19	Aragonite
C88	SO191-2 51 (8) [9] B			-49.02	3.14	Aragonite
C1	SO191-2 66 [1] A	67.8	0.351	-48.87	3.35	Aragonite
C2A	SO191-2 66 [1] B	55.6	0.229	-51.13	3.18	Aragonite
C2B	SO191-2 66 [1] B			-50.28	3.26	
C3	SO191-2 66 [1] C	81.4	0.289	-50.90	3.33	Aragonite
C92	SO191-2 66 (32) [23] B			-49.06	3.10	Aragonite *(Qtz)*
C6	SO191-2 66 (33) [16] C	55.4	0.216	-56.53	2.96	Aragonite
C7	SO191-2 66 (45) [3] B	57.3	0.399	-48.19	3.30	Aragonite *(Qtz)*
C8	SO191-2 98 (74) [21]	58.1	0.299	-47.10	3.08	Aragonite *(Qtz)*
C9	SO191-2 114 (102) [15]	56.2	0.564	-47.51	2.93	Aragonite *(Qtz)*
C10	SO191-2 124 (123) [10]	52.9	0.645	-45.85	3.91	Aragonite *(Qtz)*
C11	SO191-2 125 (124) [11]	60.5	0.423	-50.71	3.68	Aragonite *(HMC, Qtz)*
C94B	SO191-2 149 A			-42.50	2.99	Aragonite
C95	SO191-2 149 C			-30.68	2.96	
C96	SO191-2 164 [14] B			-53.29	3.25	Aragonite
C12	SO191-2 164 [14] D	64.2	0.271	-48.05	3.09	Aragonite *(Qtz)*
C13	SO191-2 165 [13] C	69.3	0.74	-47.02	3.28	Aragonite
C14A	SO191-2 165 [13] D	70.0	0.265	-48.14	3.23	Aragonite
C15	SO191-2 165 [13] E	73.0	0.296	-50.43	3.27	Aragonite
C16	SO191-3 165? C	62.1	0.309	-49.85	3.26	Aragonite
C97	SO191-3 198			-53.50	3.48	Aragonite *(Qtz)*
C20	SO191-3 St. 230 B	72.1	0.331	-44.33	2.98	Aragonite
C22A	SO191-3 238 [1]	79.5	0.233	-36.49	2.71	Aragonite *(HMC)*
C25	SO191-3 St. 290 B	57.9	0.502	-47.69	3.06	Aragonite *(Qtz)*
C26	SO191-3 316 A	69.4	0.334	-45.03	3.77	Aragonite
C27	SO191-3 238 TVG 17	70.4	0.276	-50.91	3.18	Aragonite
C4	SO191-2 66 (32) [23] C	34.7	0.339	-50.88	3.33	Aragonite *(Qtz)*
C5	SO191-2 66 (33) [16] B	36.6	0.389	-47.60	3.19	Aragonite *(Qtz)*
C19	SO191-3 229 Tray 1	42.2	0.078	-38.78	3.16	Aragonite *(HMC)*
C94A	SO191-2 149 A			1.12	2.80	Aragonite (shell)
C23	SO191-3/239 A	64.8	0.121	-19.78	6.91	Dolomite
C24	SO191-3/239 B	66.1	0.119	-20.31	6.85	Dolomite
C17	SO191-3 224 Tray 1	58.2	0.157	-21.73	6.39	Dolomite

+0.5‰ PDB for the $\delta^{18}O$ composition of New Zealand sea water (Feary et al., 1991; Crowley and Taylor, 2000), and the measured values of bottom water temperatures at the box core sites (Table 4), it is possible to constrain pore fluid compositions associated with carbonate precipitation based on the equilibrium equations for calcite (Friedman and O'Neil, 1977), aragonite (Grossman and Ku, 1986) and dolomite (Fritz and Smith, 1970), as summarised in Fig. 12. Comparing the equilibrium $\delta^{18}O$ values with measured carbonate $\delta^{18}O$ values (Table 4) shows that our calcite samples range from slightly depleted to slightly enriched with respect to regional sea water (Fig. 12A), while the aragonite precipitates and dolostones are consistently enriched by +1 to +4.5‰ PDB (Fig. 12B, C).

With respect to estimated oxygen isotopes of New Zealand marine waters, the range of depleted to enriched $\delta^{18}O$ values in the carbonates implies precipitation from evolving fluids over time. The more depleted $\delta^{18}O$ values could suggest carbonate precipitation occurred either under elevated burial temperatures (up to 20 °C and 700 m sub-bottom depth for the most depleted calcite values) or from fluids influenced by gas hydrate formation (cf. Nyman et al., this issue). We discount higher temperatures because the MDAC is clearly forming within box core penetration depths of <30 cm beneath the seafloor, where it is associated with a living chemosynthesis-based biota. Moreover, the microcrystalline texture of the aragonite samples implies diffuse flow conditions (cf. Peckmann et al., 2009) from slowly ascending fluids that likely had sufficient time to equilibrate with surrounding ambient seawater temperatures. Consequently for those MDAC samples having relatively depleted $\delta^{18}O$ values, we favour precipitation from residual fluids following the formation of gas hydrates as the heavier oxygen is preferentially incorporated into the hydrate water molecule (Davidson et al., 1983; Ussler and Paull, 1995).

By comparison, those carbonates with enriched $\delta^{18}O$ values with respect to marine waters suggest very low temperatures (<2 °C for dolomite and <0 °C for aragonite), fluids associated with local gas hydrate dissociation during precipitation, or upwards mobilisation of fluids influenced by clay mineral dehydration at depth. Low temperatures are not consistent with the present-day measured bottom water temperatures at the sample sites from c. 5° to 9 °C (Table 4). The existence of widespread methane hydrate throughout the Hikurangi Margin, and of BSRs at all sample sites (Barnes et al., 2010-this issue), is compatible with methane hydrate dissociation contributing some enriched ^{18}O to MDAC formation. However, diagenesis of volcanic ash-derived clays in subduction zones produces a smectite–illite transformation at the décollement, as well as freshened pore waters (up to $\delta^{18}O$ + 10‰ PDB) that exude from some seafloor seeps (Vrolijk, 1993; Kastner et al., 1993; Dählmann and de Lange, 2003; Hensen et al., 2004). These altered fluids migrate to the seafloor *via* mud volcanoes and along deep-seated faults (e.g. Dählmann and de Lange, 2003; Hensen et al., 2004), and hence provide a likely mechanism and source of oxygen isotope enrichment in Hikurangi Margin MDACs.

5.2.3. Co-varying trend in stable isotopic signatures of MDACs

Along the Hikurangi Margin, a parsimonious explanation for the co-varying carbon and oxygen isotope signatures (decreasing $\delta^{13}C$ and increasing $\delta^{18}O$; Fig. 9A), which also is consistent with the increasing carbonate content trend (Fig. 8), is pore fluid admixing of seawater bicarbonate, shallow microbial methane and/or thermogenic methane released from deeper in the sediment column during episodes of intermittent faulting. Fault rupture (cf. Sibson, 1994) may have triggered hydrate dissociation and/or release of deep-seated fluids freshened by clay mineral dehydration. At a given seep location,

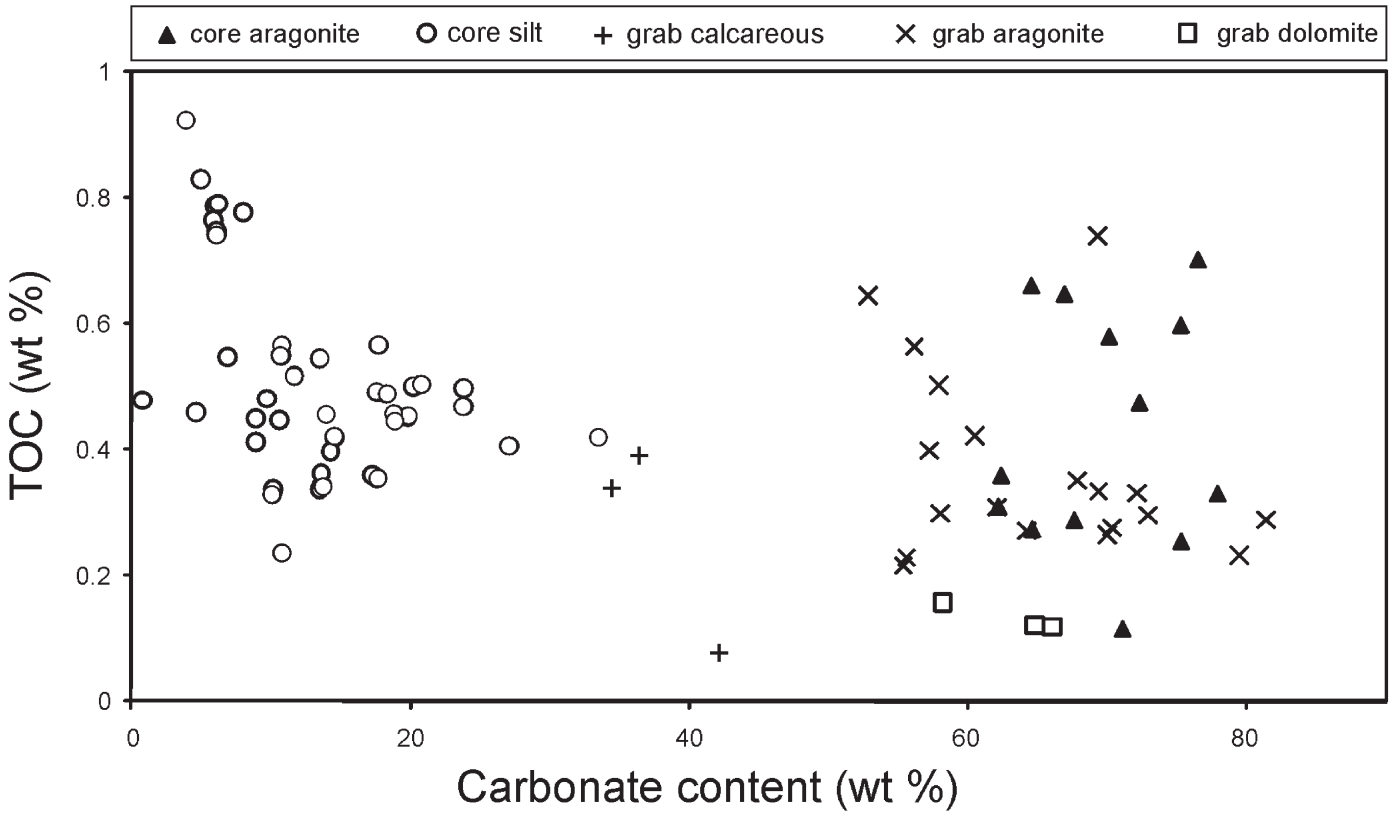

Fig. 8. Cross-plot of total organic carbon (TOC) versus carbonate content for box core sediments (i.e., carbonate-poor silts and sands – labeled 'core silt'; nodular carbonate-rich horizons – labeled 'core aragonite') and grab (rock) samples of this study. Grab samples with less than 50% calcium carbonate content are, by definition, siliciclastic sediments indurated by calcareous cement, and therefore are labeled 'grab calcareous' in the figure. They are dominantly aragonitic in mineralogy (Table 3). The other grab carbonates (≥53% calcium carbonate; Table 3) are dominated by either aragonite or dolomite mineralogy. Core samples with the highest TOC contents are from site-specific, silt-only multicores or gravity cores (Table 2). Cores with the lowest TOC contents are generally sand-rich (e.g. 66-1B; Table 2). Dolostones have very low TOC values.

pore spaces in the marine siliciclastic seabed progressively would have filled with authigenic carbonate precipitates to form indurated nodules and crusts, demarcating the influence of elevated alkalinity from AOM over time.

The co-varying stable isotopic pattern chronicled in Hikurangi Margin MDACs is widespread amongst other methane seep provinces, and therefore probably indicates broadly comparable seafloor biogeochemical and hydrogeologic processes functioning during seep field development. Examples include the Cascadia margin offshore Oregon (group II carbonates of Kulm and Suess, 1990; group E carbonates of Greinert et al., 2001); Florida Escarpment (Paull et al., 1992); Nankai Trough, Japan (Sakai et al., 1992); northern Gulf of Mexico (Roberts and Aharon, 1994); eastern Mediterranean Sea mud volcanoes (Aloisi et al., 2000); Blake Ridge diapir (Naehr et al., 2000); the Eel River margin, offshore northern California (group A bulk sedimentary carbonates of Orphan et al., 2004); and Jiulong methane reef, South China Sea (Han et al., 2008). Studies bearing the closest isotopic and mineralogic similarities to the Hikurangi Margin data set are those that analysed the bulk fine-fraction carbonate within unconsolidated sediments as well as the indurated nodules and bands which formed within the same sediments (e.g. Fig. 9B). This relatively widespread geochemical feature of seep-carbonates suggests similar processes operating at several locations worldwide in the transformation of near-seafloor sediments to indurated MDACs. Some modern (e.g. von Rad et al., 1996) and fossil (e.g. Mazzini et al., 2003; Svensen et al., 2003) seep-carbonate examples display an analogous, co-varying stable isotopic trend in stable isotopes, but with a shift towards marked depletion in $\delta^{18}O$ signatures (to −20‰ PDB). These negative $\delta^{18}O$ values also correspond to samples with more positive $\delta^{13}C$ values measured for a given setting. Negative oxygen isotopes likely indicate meteoric fluid inputs, elevated formation temperatures, or diagenetic overprinting by burial fluids, the last a signal typical for many older Phanerozoic seep-carbonates worldwide (Campbell, 2006). Some other modern studies have reported greatly scattered isotopic groupings for particular methane seep provinces (e.g. Monterey Bay – Stakes et al., 1999; Hydrate Ridge – Greinert et al., 2001; Costa Rica margin – Han et al., 2004). Notably these provinces also include carbonates of different ages, fluid contents and/or tectonosedimentary origins distinct from seep regions that have yielded only samples indicative of seafloor-related, sulphate dependent AOM.

Numerical modeling has shown that authigenic aragonitic crusts of several centimetres thickness, typical of many modern seep provinces including the Hikurangi Margin, form at the sediment–water interface or within near-seafloor sediments under a narrow range of physical and biogeochemical conditions (Luff et al., 2004). Specifically, crusts develop within a few hundred years where there is sufficient supply of dissolved methane (>50 mM), relatively low bioturbation rates, and upward pore fluid-flow velocities of 20–60 cm/yr (Luff et al., 2004). The crusts essentially form at the seabed. Thus, where they are found as multiple horizons within a sedimentary succession in a seep region, such as within the thick (60 m) ODP Site 966 cores drilled over the Blake Ridge diapir (Fig. 9B), those crusts now situated deep within the sedimentary column represent former positions of the seafloor during episodic sedimentation and seepage. Naehr et al. (2000) noted a +1‰ shift in oxygen isotopes from authigenic carbonate nodules sampled at particular depth intervals in their ODP core (cf. Fig. 9B), which they suggested correlated with the isotopic composition of past glacial bottom waters. In comparison, our carbonate samples were not

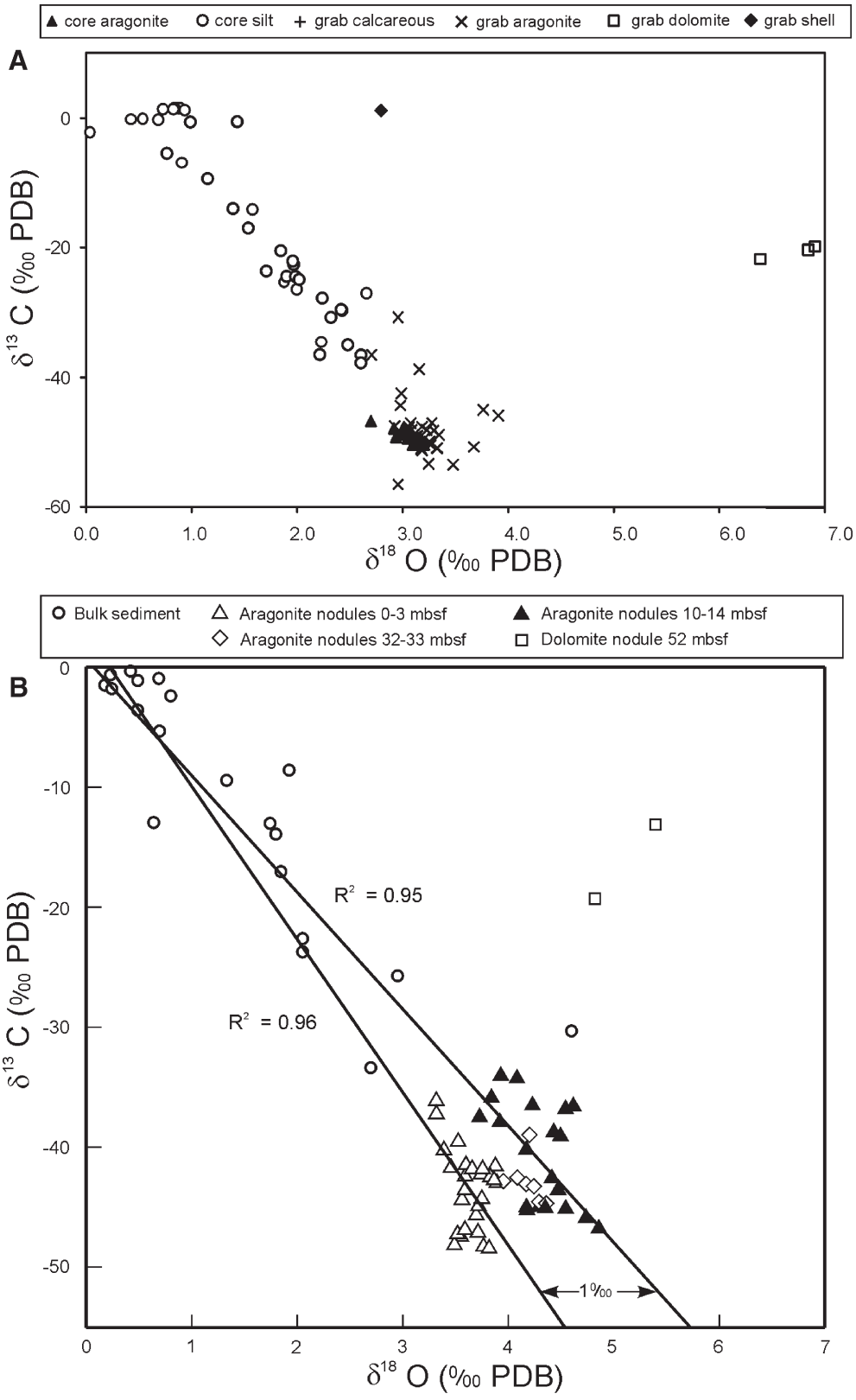

Fig. 9. Cross-plot of stable carbon and oxygen isotopes for box core and grab sample carbonates from the convergent Hikurangi Margin (A) compared to those from an ODP core collected at the Blake Ridge diapir of the offshore eastern U.S. passive margin (B) (Naehr et al., 2000). (A) For unconsolidated box core silt/sand samples (open circles), $\delta^{13}C$ and $\delta^{18}O$ values were measured from bulk fine-fraction (<100 μm) carbonates. Three isotopic groupings are evident: shell, dolostone, and largely aragonitic and grab carbonates, the last of which plot in a linear trend between those derived from seawater bicarbonate (carbon and oxygen values around 0‰ PDB) and those sourced from sulphate-dependent AOM in near seabed (shallow subsurface) conditions. (B) Isotope data from several thin aragonite horizons interbedded with siliciclastic sediments in a composite 60 m core above the Blake Ridge diapir (ODP Site 996) represent former seafloor positions during past methane seepage (Redrawn from Naehr et al., 2000). The +1‰ PDB $\delta^{18}O$ shift shown in carbonate horizons from 10–14 mbsf is inferred as influenced by past glacial bottom waters.

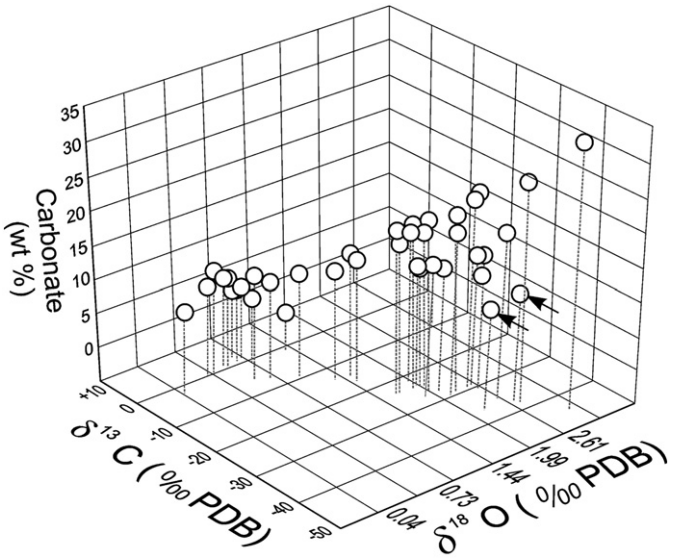

Fig. 10. Three-dimensional box plot of carbonate content *vs* $\delta^{13}C$ and $\delta^{18}O$ from unconsolidated bulk fine-fraction carbonate in Hikurangi Margin core samples. The data show an increase in $\delta^{18}O$ and carbonate content with decreasing $\delta^{13}C$. Data points are more widely spread for $\delta^{13}C$ values more negative than −20‰ PDB, and may demarcate natural seabed heterogeneity (porosity, permeability), hydrogeologic variability in methane-charged fluid flux to the seafloor, or potentially different past bottom water temperatures (cf. Naehr et al., 2000; Liebetrau et al., 2010-this issue). Arrows label the most sand-rich unconsolidated sediment samples, which yielded unusually low carbonate contents.

dated, but some samples from other Hikurangi Margin seep-carbonate blocks have a reported age range between 12,400 yrs BP and the present-day (Liebetrau et al., 2010-this issue). Thus, some New Zealand MDACs also may have precipitated under cooler glacial conditions.

5.3. Lithologic and biotic affiliations at Hikurangi Margin seeps

The lithologic and biotic groupings identified in Hikurangi Margin samples show that these hydrocarbon seep-carbonates have formed with discrete infaunal and epifaunal associations. Furthermore, some carbonates record development at different times and/or under different physicochemical conditions, including relict seepage from a distinct diagenetic regime. Three clear groupings are evident.

5.3.1. Diffuse seepage-related, softground megafauna in box cores

The variably calcareous, siliciclastic sandy silts to silty sands in the box cores contain a softground mega-invertebrate biota, in particular a shallow infaunal and semi-infaunal/epifaunal affiliation (Fig. 6). Some of these shelly taxa were cemented into denser carbonate bands (to c.15 cm thick) by AOM-produced alkalinity within sedimentary pore spaces. Chemosymbiotic bivalve taxa include infaunal *Lucinoma* and *Acharax*, and the semi-infaunal/epifaunal *Calyptogena*, which together constitute the bulk of the megafaunal biomass. Associated mega-invertebrates include scattered siboglinid tubeworms, carnivorous gastropods (*Nassarius*, *Falsilunatia*, *Acteon*), and small *Provanna*, a seep-related gastropod which grazes upon sulphur oxidising *Beggiatoa* mats at other modern seeps (Levin and Michener, 2002; Sahling et al., 2002). Similar lucinid, solemyid and vesicomyid assemblages are known from other settings marginal to main vent areas, in waning flow conditions, or at ephemeral seeps with low pore water sulphide concentrations (e.g. Sibuet et al., 1988; MacDonald et al., 1990; Carney, 1994; Sibuet and Olu, 1998; Suess et al., 1998; Callender and Powell, 2000; Sahling et al., 2002, 2003; Treude et al., 2003; Sellanes et al., 2008). The mineralogy and stable isotopes of the affiliated MDACs suggest precipitation took place near or at the sediment surface in dysoxic environments, with high sulphate concentrations and high total alkalinity (e.g. group E of Greinert et al., 2001; cf. Burton, 1993; Savard et al., 1996; Peckmann et al., 2001; Han et al., 2004; Teichert et al., 2005a).

Broken shells of *Calyptogena* sp. commonly are incorporated into cemented horizons of the Hikurangi Margin box cores (e.g. Fig. 5). *Calyptogena* sp. also occurs articulated and in life position amongst scattered carbonate nodules in the host silts, in places with dense nodular carbonate bands directly beneath them (e.g. Figs. 3C and 5B). Shallow subsurface carbonate formation is known to take place under *Calyptogena* beds at other modern seeps, where active clam pumping causes downwelling of seawater sulphate which meets upwardly diffusing methane in a mixing zone c.10–35 cm bsf (e.g. Henry et al., 1992; Wallmann et al., 1997; Tryon et al., 2002; Luff et al., 2004; Orphan et al., 2004). Consequently, bioirrigation affects solute transport rate and pore water chemistry, and shifts the locus of authigenic carbonate precipitation downward into the seabed (cf. Wallmann et al., 1997; Luff et al., 2004; Sommer et al., 2006).

The occurrence of juvenile *Acharax* in bioturbated silts overlying carbonate-cemented *Calyptogena* (e.g. box core slab 98-2B, Figs. 2C and 5A) is inferred to imply waning fluid flow through time. Only one u-shaped solemyid dwelling tube (*Solemyatuba*) was noted ('ub' in Fig. 5A). Most *Acharax* burrow morphologies (cf. *Planolites*?) in the box core indicate active horizontal movement within the silts (horizon B of Fig. 2C), possibly produced while the clam was searching for low-concentration sulphide patches in the unconsolidated sediment (cf. Treude et al., 2003). Similar in thickness to the depth profile of the *A. clarificata* horizon in box core 98-2B (Fig. 5A), low-sulphide sedimentary layers (c.15 cm thick, 0.1 to 0.3 mM H_2S) characterise Hydrate Ridge solemyid communities (Sahling et al., 2002). Treude et al. (2003) also reported that *Acharax* fields at Hydrate Ridge are sometimes

Fig. 11. Total ion chromatograms of sylilated total EOMs of aragonitic grab samples (A) SO191-3 St.230 A and (B) SO191-2 124(123) [10], and a dolostone grab sample (C) SO191-3 239. Cr: crocetane; Cr:1: mono-unsaturated crocetenes; Ph: Phytane; IS: Internal standard; PMI: 2,6,10,15,19-pentamethylicosane; PMI:x: unsaturated PMIs with x double bonds ($x = 1$ to 4); DGD: Non-isoprenoidal dialkyl glycerol diethers; T: Tetrahymanol; C32H-OTMS: silylated C_{32} hopanol; GME: Glycerol monoether; A: Alkenone; $C_{27}\Delta^{5,22}$ = Cholesta-5,22-dien-3 Δ-ol; C_{28} $\Delta^{5,22}$ = 24-methylcholesta-5,22-dien-3 Δ-ol; C_{29} Δ^{5} = 24-ethylcholest-5-en-3 Δ-ol. Cn:m refers to n carbon numbers and m double bonds for the compound considered. *N*-alkanols, *n*-alkanoic acids and *n*-alkanes are indicated by their carbon number and the respective symbols ●, ▼ and ◆.

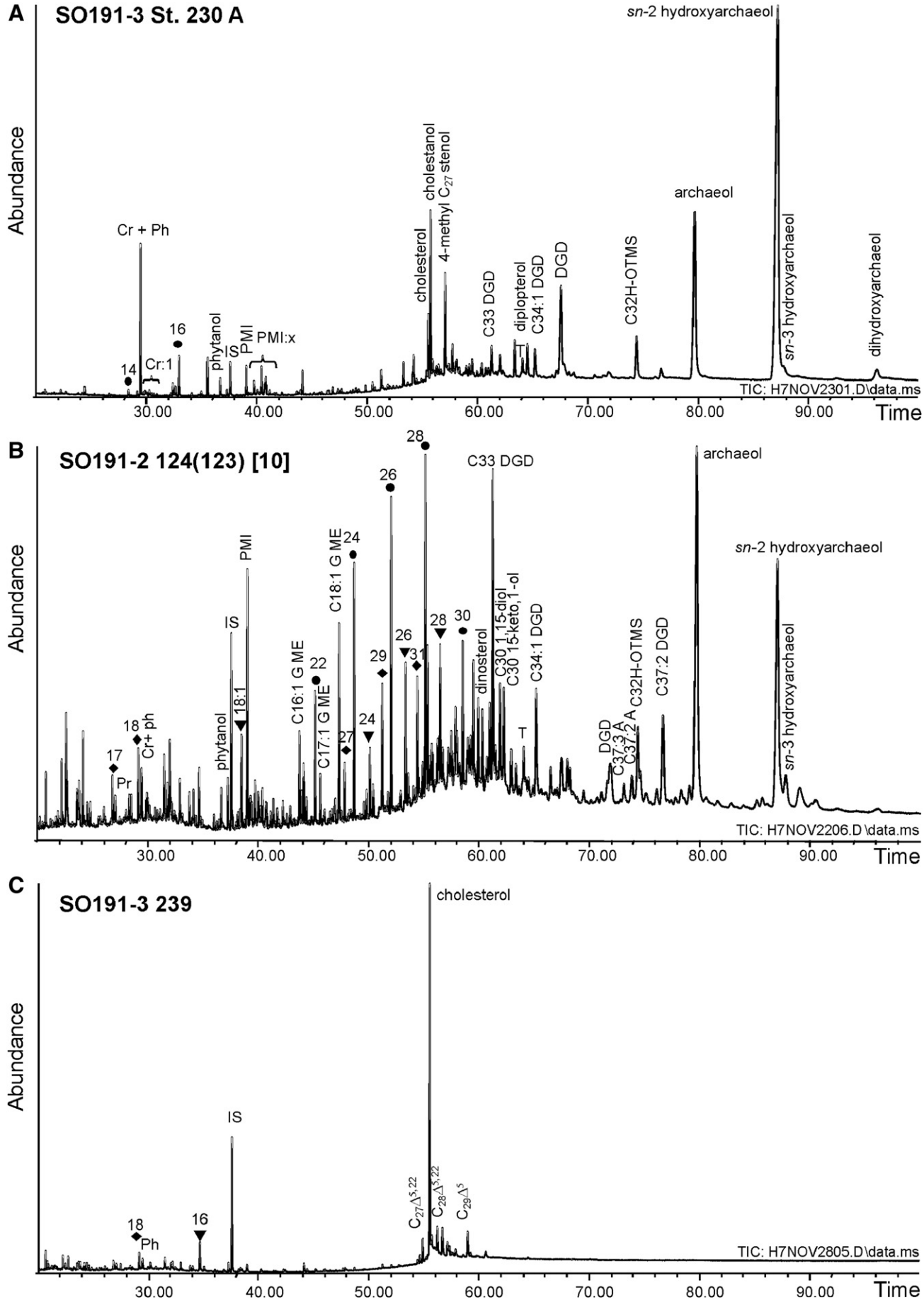
A
SO191-3 St. 230 A
Abundance
Cr + Ph
14
Cr:1
16
phytanol
IS
PMI
PMI:x
cholesterol
cholestanol
4-methyl C27 stenol
C33 DGD
diplopterol
C34:1 DGD
DGD
C32H-OTMS
archaeol
sn-2 hydroxyarchaeol
sn-3 hydroxyarchaeol
dihydroxyarchaeol
TIC: H7NOV2301.D\data.ms
30.00 40.00 50.00 60.00 70.00 80.00 90.00 Time
B
SO191-2 124(123) [10]
Abundance
17
Pr
18
Cr+ ph
phytanol
IS
18:1
PMI
C16:1 G ME
C17:1 G ME
22
C18:1 G ME
24
27
29
26
28
31
30
C33 DGD
dinosterol
C30 1,15-diol
C30 15-keto,1-ol
C34:1 DGD
T
DGD
C37:3 A
C37:2 A
C32H-OTMS
C37:2 DGD
archaeol
sn-2 hydroxyarchaeol
sn-3 hydroxyarchaeol
TIC: H7NOV2206.D\data.ms
30.00 40.00 50.00 60.00 70.00 80.00 90.00 Time
C
SO191-3 239
Abundance
18
Ph
16
IS
cholesterol
C27Δ5,22
C28Δ5,22
C29Δ5
TIC: H7NOV2805.D\data.ms
30.00 40.00 50.00 60.00 70.00 80.00 90.00 Time

Table 4
Oxygen isotope values for carbonate precipitated in equilibrium with seawater at the temperatures measured at the three study sites (Faure et al., 2010-this issue), and the range of $\delta^{18}O$ values measured in the carbonate samples.

Location	Omakere Ridge/Opouawe Bank	Rock Garden
Temp range °C	4.4 to 5.6	7.4 to 8.7
Calcite		
$\delta^{18}O_{calcite}$ ‰ PDB (In equilibrium with seawater)	1.5 to 2.75	0.75 to 2
$\delta^{18}O_{calcite}$ ‰ PDB (Measured sample)	0 to 3	0 to 3
Aragonite		
$\delta^{18}O_{aragonite}$ ‰ PDB (In equilibrium with seawater)	0.75 to 2	0 to 1.25
$\delta^{18}O_{aragonite}$ ‰ PDB (Measured sample)	2.8 to 4	2.8 to 4
Dolomite		
$\delta^{18}O_{dolomite}$ ‰ PDB (In equilibrium with seawater)		3.5 to 4.7
$\delta^{18}O_{dolomite}$ ‰ PDB (Measured sample)		6 to 7

underlain by *Calyptogena* shells deeper in the sediments, suggesting changing seep-fluid distributions over time. Furthermore, the common occurrence of articulated *Lucinoma galathea* in several cores from the Hikurangi Margin also implies low pore water sulphide concentrations. This chemosymbiotic bivalve, like *Acharax*, is not associated with high-flux vent areas in other seep regions (Van Dover, 2000). In fossil seep deposits, lucinid bivalves are typical of 'diffuse' or marginal fluid-flow facies (e.g. Clari et al., 1994; Kauffman et al., 1996; Nesbitt and Campbell, 2004; Campbell et al., 2008).

5.3.2. Chemosymbiotic epifauna associated with fresh grab samples of near-vent areas

The biota associated with the light coloured, unweathered, aragonitic micarb grab samples include seep-related, epifaunal bathymodiolin bivalves, tubeworms, sponges and limpets living atop seafloor hardgrounds, some of which became encased within the forming carbonates (cf. Fig. 7A–L). As at other seep sites (e.g. MacDonald et al., 1990; Barry et al., 1997; Van Dover et al., 2003), the mussel-dominated carbonate samples (e.g. Fig. 7H, J) are distinct from blocks of cemented vesicomyids (e.g. Fig. 2A, B), implying that the two megafaunal assemblages do not commonly co-exist. Tubeworms occur scattered about mussel and vesicomyid shell accumulations. At Barbados seeps, Olu et al. (1996) inferred that vesicomyid clams are the first colonisers of soft sediments, followed by later recruitment of bathymodiolin mussels as sediment lithification proceeded and fluid flow rates increased. Barry et al. (1997) noted the lack of mussels at Monterey Bay seeps, which constitutes a low fluid-flux seep province. They suggested that methanotrophy restricts mussels to seeps with a constant supply of methane to the seafloor (i.e. near vents). By contrast, vesicomyids store sulphur for use in endosymbiotic sulphide oxidation, giving these clams a selective advantage in low-sulphide, soft-bottom seep settings (Barry et al., 1997). In our small grab sample set from Hikurangi Margin seeps at Rock Garden, living *Bathymodiolus tangaroa* was found attached to carbonate hardgrounds composed of cemented mussel-shell hash (Fig. 7H), along with a seep-restricted assemblage of siboglinid tubeworms, methanotrophic suberitid sponges and limpets, all suggestive of active, sustained seepage at this location (cf. Thurber et al., 2010-this issue). Both mussel and vesicomyid shell hashes have been reported adjacent to their respective living communities elsewhere, with piles of disarticulated shells attributed to massive die-offs potentially associated with dramatic local fluctuations in seep-fluid fluxes (Van Dover et al., 2003).

With regard to tubeworm–carbonate associations in particular, we found no evidence for tubeworms "boring" into carbonate (cf. Sassen et al., 2004), but rather they were lodged amongst shells in unconsolidated sediments (e.g. Fig. 3A, B), cemented in life position (Fig. 7 K; cf. Luff et al., 2004; Campbell et al., 2008), or anchored to rock with the tapering distal ends intertwined through the open framework of the carbonate (Fig. 7C; cf. Carney, 1994). Many Hikurangi Margin seep-carbonate samples are rife with holes, derived from several sources: (1) the present-day boring epifauna on seep-carbonate hardgrounds; (2) previously formed burrows (e.g. Fig. 6P) in originally soft sediments; and (3) fluid conduits that maintained primary porosity within the cementing seabed (cf. Teichert et al., 2005a; Han et al., 2008). In some samples, empty tubes that mimic the dimensions and morphology of siboglinid tubeworms are overgrown by white aragonite cements (Fig. 7 K), an association linked in other modern and fossil studies to near-vent, strongly advective, methane-rich fluid flow (cf. Campbell et al., 2002, 2008; Han et al., 2004; Haas et al., 2009a,b; Peckmann et al., 2009).

5.3.3. Exhumed carbonate hardgrounds with deep-sea epifauna

The third biota-carbonate grouping is quite unlike the other Hikurangi Margin examples with respect to faunal associations, mineralogy and isotopes. These dolostones show clear signs of long-term seafloor exposure and weathering, such as well-developed Fe/Mn crusts, dissolution pits, extensive marine borings (cf. Stakes et al., 1999; Campbell et al., 2008), and a diverse non-seep epifauna (e.g. Fig. 7 L–O). Similar heterotrophic taxa have been reported at seeps elsewhere, where access to carbonate hardgrounds appears to be more important than enhanced nutrient availability from local chemosynthetic production (e.g. Jensen et al., 1992; Sellanes et al., 2008). For example, corals (Fig. 7 N) are well-known hardground colonisers of deep-sea carbonates of methane seep origin, both modern and fossil (e.g. MacDonald et al., 1989; Hovland and Risk, 2003; Goedert and Peckmann, 2005), and including the Hikurangi Margin (Campbell et al., 2008; Liebetrau et al., 2010-this issue). Baco et al. (2010-this issue) reports antipatherian, gorgonian, sylasterid and scleractinian corals from Rock Garden, where several of our dolostone blocks were collected.

The mineralogy of the Hikurangi Margin dolostones may indicate that their development occurred relatively deeper in the sediment column than the aragonitic MDACs, as is also inferred from similar examples from other seep provinces (e.g. Hydrate Ridge, Greinert et al., 2001; Costa Rican margin, Han et al., 2004; Monterey Bay, Stakes et al., 1999). The fact that lipid biomarker analysis of the Hikurangi Margin dolostones does not show any of the archeal lipids commonly associated with AOM is consistent with this hypothesis. To find such weathered and iron-stained carbonates exposed on the seafloor today requires uplift and exhumation to the seafloor following their formation, conditions reasonably expected in an active thrust-fault regime such as that found offshore eastern North Island today (Barnes et al., 2010-this issue). At Hydrate Ridge, isotopically similar dolostones imply formation at the deep SRZ/methanogenesis boundary (i.e., moderately depleted $\delta^{13}C$ of −26 to −32‰ PDB and enriched $\delta^{18}O$ of +6.5 to +7.5‰ PDB in group B samples of Greinert et al., 2001).

The Hikurangi Margin dolostones also are isotopically similar to Miocene-age tubular concretions exposed onshore (e.g. Fig. 1) at Cape

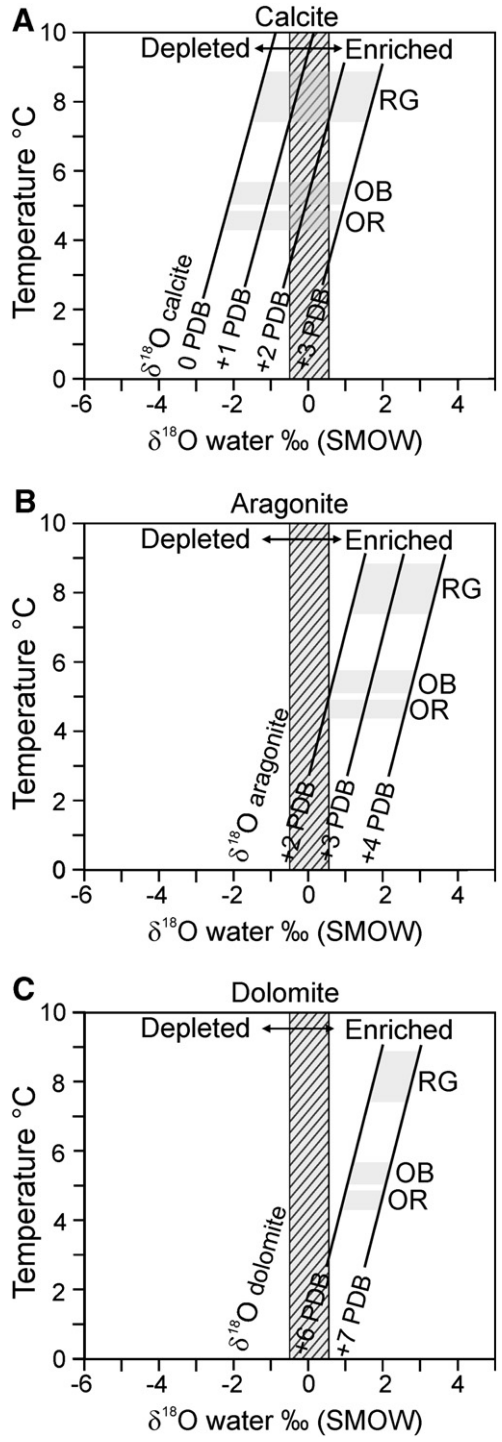

Fig. 12. Possible water compositions (SMOW) responsible for carbonate precipitation at Omakere Ridge (OR), Opouawe Bank (OB) and Rock Garden (RG) seep sites. The grey highlighted regions mark early 2007 temperature measurements from each study site. The grey hatched rectangle corresponds to estimated marine water compositions. Curves crossing the grey hatched region to the left of the dashed line are depleted with respect to marine seawater. Curves crossing to the right of the dashed line are enriched with respect to marine seawater. (A) Equilibrium diagram for calcite based on equations from Friedman and O'Neil (1977); (B) aragonite equilibrium diagram based on equations from Grossman and Ku (1986); and (C) dolomite equilibrium calculation diagram based on equations from Fritz and Smith (1970).

Turnagain (Nyman et al., 2010-this issue), East Cape and Taranaki (Nyman, 2009), North Island, New Zealand. These widespread tubular concretions within deep-water mudstones are the inferred fossil 'fluid plumbing' conduits of 7–10 Ma methane seep systems. For the offshore dolostones of this study, $\delta^{13}C$ values of around −20‰ PDB may have been sourced from a shallow subsurface methane pool that had experienced extensive oxidation (>80%, cf. Whiticar, 1999; from a biogenic methane source of c. −60‰ PDB, cf. Faure et al., 2010-this issue). Subsequent uplift and exhumation of overlying soft sediments then may have exposed the Hikurangi Margin dolostones to seafloor dissolution, iron staining, deep-sea boring organisms and heterotrophic epibiont colonisation, which have significantly modified the surfaces of these blocks.

Hence, it appears that complex interactions occur in seep provinces amongst active tectonism/uplift, diapirism, slumping, migrating fluids, sedimentation and erosion, which ultimately juxtapose carbonates of different fluid sources, origination depths and ages on the present-day seafloor (cf. Stakes et al., 1999; Naehr et al., 2007). Certainly in the case of the Hikurangi Margin grab carbonate samples, fresh and weathered blocks display distinctly different mineralogies, textures, isotopes, and affiliated biota, thus implying a temporal (cf. Liebetrau et al., 2010-this issue) and/or spatial disparity in their formation environments and post-formation histories.

6. Conclusions

Cores and grab samples collected during RV SONNE cruise SO191 offshore eastern North Island, New Zealand, targeted authigenic carbonates at seep sites. They yielded three biotic-carbonate associations. Cores revealed a low-sulphide, largely chemosymbiotic and infaunal, soft-bottom bivalve affiliation (*Calyptogena*, *Lucinoma*, and *Acharax*) within layered silt, fine sand and nodular, microcrystalline aragonite bands. Fresh-appearing, texturally varied grab carbonates are dominantly aragonitic, and host epifaunal, seep-related taxa typical of steady methane and sulphide supply, such as chemosymbiotic mussels, methanotrophic sponges, and tubeworms. A third biotic-carbonate grouping constitutes grab samples of weathered, iron-stained, bored, microcrystalline dolostones, encrusted by a non-seep epifauna from adjacent deep-sea habitats. Stable carbon and oxygen isotopic signatures of the core and grab aragonitic samples (depletion in $\delta^{13}C$ to −50‰ PDB), as well as lipid biomarker distributions, indicate formation in shallow seabed areas of microbially induced, sulphate-dependent AOM. By contrast, the dolostones are moderately depleted in $\delta^{13}C$ to −20‰ PDB, suggesting oxidation of a biogenic methane reservoir at depth, perhaps at the base of the SRZ. With respect to estimated $\delta^{18}O_{seawater}$ and bottom water temperatures measured at the study sites, depleted oxygen isotope values of the Hikurangi Margin carbonates imply temperature variations or episodes of gas hydrate formation. Carbonates enriched in $\delta^{18}O$ suggest very cold bottom waters (< 2 °C), possible influence from gas hydrate dissociation, or pore fluid freshening by clay mineral dehydration. A clear isotopic trend of decreasing $\delta^{13}C$ and increasing $\delta^{18}O$ and carbonate content of Hikurangi Margin samples delineates admixing amongst fluids derived from seawater bicarbonate, biogenic methane and/or thermogenic methane. Similar trends have been reported from modern seeps elsewhere, confirming that the seep-carbonate record captures the heterogeneous but steady initiation and development of methane seepage around many parts of the world's continental margins.

Acknowledgements

We thank the Captain and crew of *RV SONNE* for their expertise and assistance, and Lindsey White and Ruth Martin for shipboard sampling. The cruise was funded by the German Federal Ministry for Education and Research within the project COMET: COntrols on METhane fluxes and their climatic relevance in marine gas hydrate-bearing sediments (grant nos. 03G0191A and 03G0600D). Analytical costs were borne by a research grant to KAC and CSN from the Marsden Fund Council for government funding, administered by the Royal Society of New Zealand,

and by IFM-GEOMAR, Kiel, Germany. Appreciation is also extended to the Auckland Radiology Group, Bruce Marshall, John Wilmshurst, Louise Cotterall, Dave Francis, Neel Jinadasa, Sarah Ewen, Bettina Domeyer, and Ben Andrew for discussions, and analytical or taxonomic assistance. EG and GAL publish with the permission of the Executive Director, Geoscience Australia. JG acknowledges the EU for financial support and the opportunity to work at GNS Science and RCMG through a Marie Curie grant (MOIF-CT-2005-007436). This is publication no. GEOTECH-1223 of the R&D program GEOTECHNOLOGIEN. Alan Orpin, Ruth Martin and Erwin Suess provided comments that greatly improved the quality of the manuscript.

References

Aharon, P., 2000. Microbial processes and products fueled by hydrocarbons at submarine seeps. In: Riding, R.E., Awramik, S.M. (Eds.), Microbial Sediments. Springer-Verlag, Berlin, pp. 270–281.

Aloisi, G., Pierre, C., Rouchy, J.-M., Foucher, J.-P., Woodside, J., Scientific Party, M.E.D.I.N. A.U.T., 2000. Methane-related authigenic carbonates of eastern Mediterranean Sea mud volcanoes and their possible relation to gas hydrate destabilization. Earth Planet. Sci. Lett. 184, 321–338.

Aloisi, G., Bouloubassi, I., Heijs, S.K., Pancost, R.D., Pierre, C., Sinninghe Damsté, J.S., Gottschal, J.C., Forney, L.J., Rouchy, J.-M., 2002. CH_4-consuming microorganisms and the formation of carbonate crusts at cold seeps. Earth Planet. Sci. Lett. 203, 195–203.

Baco, A.R., Rowden, A.A., Levin, L.A., Smith, C.R., Bowden, D., RENEWZ I cruise scientific party, 2010. Initial characterization of cold seep faunal communities on the New Zealand margin. Mar. Geol. 272, 251–259 (this issue).

Barnes, P.M., Lamarche, G., Bialas, J., Henrys, S., Pecher, I., Netzeband, G.L., Greinert, J., Mountjoy, J.J., Pedley, K., Crutchley, G., 2010. Tectonic and geological framework for gas hydrates and cold seeps on the Hikurangi subduction margin, New Zealand. Mar. Geol. 272, 26–48 (this issue).

Barry, J.P., Kochevar, R.E., Baxter, C.H., 1997. The influence of pore-water chemistry and physiology on the distribution of vesicomyid clams at cold seeps in Monterey Bay: implications for patterns of chemosynthetic community organization. Limnol. Oceanogr. 42, 318–328.

Blott, S., Pye, K., 2001. GRADISTAT: a grain size distribution and statistics package for the analysis of unconsolidated sediments. Earth Surf. Process. Landforms 26, 1237–1248.

Blumenberg, M., Seifert, R., Reitner, J., Pape, T., Michaelis, W., 2004. Membrane lipid patterns typify distinct anaerobic methanotrophic consortia. Proc. Nat. Acad. Sci. 101, 11111–11116.

Boetius, A., Ravenschlag, K., Schubert, C.J., Rickert, D., Widdel, F., Gieskes, A., Amann, R., Jørgensen, B.B., Witte, U., Pfannkuche, O., 2000. A microbial consortium apparently mediating anaerobic oxidation of methane. Nature 407, 623–626.

Bohrmann, G., Greinert, J., Suess, E., Torres, M., 1998. Authigenic carbonates from the Cascadia subduction zone and their relation to gas hydrate stability. Geology 26, 647–650.

Boyd, S., 2009. Benthic invertebrate assemblages and sediment characteristics of cold seeps on the Hikurangi Margin, New Zealand. Auckland University of Technology, Auckland. 208 pp.

Burton, E.A., 1993. Controls on marine carbonate cement mineralogy: review and reassessment. Chem. Geol. 105, 163–179.

Callender, W.R., Powell, E.N., 2000. Long-term history of chemoautotrophic clam-dominated faunas of petroleum seeps in the northwestern Gulf of Mexico. Facies 43, 177–204.

Campbell, K.A., 2006. Hydrocarbon seep and hydrothermal vent paleoenvironments: past developments and future research directions. Palaeoecol. Palaeogeogr. Palaeoclimat. 232, 362–407.

Campbell, K.A., Farmer, J.D., Des Marais, D., 2002. Ancient hydrocarbon seeps from the Mesozoic convergent margin of California: carbonate geochemistry, fluids and paleoenvironments. Geofluids 2, 63–94.

Campbell, K.A., Francis, D.A., Collins, M., Gregory, M.R., Nelson, C.S., Greinert, J., Aharon, P., 2008. Hydrocarbon seep-carbonates of a Miocene forearc (East Coast Basin), North Island, New Zealand. Sed. Geol. 204, 83–105.

Carney, R.S., 1994. Consideration of the oasis analogy for chemosynthetic communities at Gulf of Mexico hydrocarbon vents. Geo Mar. Lett. 14, 149–159.

Clari, P., Fornara, L., Ricci, B., Zuppi, G.M., 1994. Methane-derived carbonates and chemosymbiotic communities of Piedmont (Miocene, northern Italy): an update. Geo Mar. Lett. 14, 201–209.

Clari, P., Dela Pierre, F., Martire, L., Cavagna, S., 2009. The Cenozoic CH_4-derived carbonates of Monferrato (NW Italy): a solid evidence of fluid circulation in the sedimentary column. Mar. Geol. 265, 167–184.

Claypool, G.E., Kaplan, I.R., 1974. The origin and distribution of methane in marine sediments. In: Kaplan, I.R. (Ed.), Natural Gases in Marine Sediments. Plenum Publishing Corporation, New York, pp. 99–139.

Crowley, S.F., Taylor, P.D., 2000. Stable isotope composition of modern bryozoan skeletal carbonate from the Otago Shelf, New Zealand. N. Z. J. Mar. Freshw. Res. 34, 331–351.

Dählmann, A., de Lange, G.J., 2003. Fluid–sediment interactions at eastern Mediterranean mud volcanoes: a stable isotope study from ODP Leg 160. Earth Planet. Sci. Lett. 212, 377–391.

Davidson, D.W., Leaist, D.J., Hesse, R., 1983. Oxygen-18 enrichment in water of a clathrate hydrate. Geochim. Cosmochim. Acta 47, 2293–2295.

Davies, E.J., Frederick, J.B., Leask, W.L., Williams, T.J., 2000. East Coast drilling results. Proc. N. Z. Petrol. Conf, pp. 101–113.

De Mets, C., Gordon, R.G., Argus, D.F., Stein, S., 1990. Current plate motions. Geophys. J. Int. 101, 425–478.

Faure, K., Greinert, J., Pecher, I.A., Graham, I.J., Massoth, G.J., Ronde, C.E.J.D., Wright, I.C., Baker, E.T., Olson, E.J., 2006. Methane seepage and its relation to slumping and gas hydrate at the Hikurangi Margin, New Zealand. N. Z. J. Geol. Geophys. 49, 503–516.

Faure, K., Greinert, J., Schneider von Deimling, J., McGinnis, D.F., Kipfer, R., Linke, P., 2010. Methane seepage along the Hikurangi margin of New Zealand: geochemical and physical data from the water column, sea surface and atmosphere. Mar. Geol. 272, 170–188 (this issue).

Feary, D.A., Davies, P.J., Pigram, C.J., Symonds, P.A., 1991. Climatic evolution and control on carbonate deposition in northeast Australia. Palaeogeogr. Palaeoclimat. Palaeoecol. 89, 341–361.

Folk, R.L., Ward, W.C., 1957. Brazos River bar: a study in the significance of grain size parameters. J. Sed. Petrol. 27, 3–26.

Francis, D.A., 1998. Gas chromatograph and isotope analyses of gas seeps, PEPs 38330, 38328, 38332 and former 38312, East Coast Basin. Open File Report 3111, 10 p.

Friedman, I., O'Neil, J.R., 1977. Compilation of stable isotope fractionation factors of geochemical interest. In: Fleisher, M. (Ed.), U.S. Geol. Survey Prof. Paper vol. 440.

Fritz, P., Smith, D.G.W., 1970. The isotopic composition of secondary dolomite. Geochim. Cosmochim. Acta 34, 1161–1173.

Goedert, J.L., Peckmann, J., 2005. Corals from deep-water methane-seep deposits in Paleogene strata of western Oregon and Washington, U.S.A. In: Friewald, A., Roberts, J.M. (Eds.), Cold-Water Corals and Ecosystems. Springer-Verlag, Berlin, pp. 27–40.

Greene, H.G., Maher, N., Naehr, T.H., Orange, D.L., 1999. Fluid flow in the offshore Monterey Bay region. In: Garrison, R.E., Aiello, I.W., Moore, J.C. (Eds.), Late Cenozoic Fluid Seeps and Tectonics along the San Gregorio Fault Zone in the Monterey Bay Region. Pac. Sec. AAPG Vol. and Guidebook GB-76, pp. 1–19.

Greinert, J., Bohrmann, G., Suess, E., 2001. Gas-hydrate-associated carbonates and methane-venting at Hydrate Ridge: classification, distribution, and origin of authigenic carbonates. In: Paull, C.K., Dillon, P.W. (Eds.), Natural Gas Hydrates: Occurrence, Distribution, and Detection: AGU, Geophys. Monogr., 124, pp. 99–113.

Greinert, J., Lewis, K., Bialas, J., Pecher, I., Rowden, A., Bowden, D.A., De Batist, M., Linke, P., 2010. Methane seepage along the Hikurangi Margin, New Zealand: Overview of studies in 2006 and 2007 and new evidence from visual, bathymetric and hydroacoustic investigations. Mar. Geol. 272, 6–25 (this issue).

Grosjean, E., Logan, G.A., 2007. Incorporation of organic contaminants into geochemical samples and an assessment of potential sources: examples from Geoscience Australia marine survey S282. Org. Geochem. 38, 853–869.

Grossman, E.L., Ku, T.-L., 1986. Oxygen and carbon isotope fractionation in biogenic aragonite: temperature effects. Chem. Geol. 59, 59–74.

Haas, A., Little, C.T.S., Sahling, H., Bohrmann, G., Himmler, T., Peckmann, J., 2009a. Mineralization of vestimentiferan tubes at methane seeps on the Congo deep sea fan. Deep Sea Res. I 56, 283–293.

Haas, A., Little, C.T.S., Sahling, H., Bohrmann, G., Himmler, T., Peckmann, J., 2009b. Mineralization of vestimentiferan tubes at methane seeps on the Congo deep sea fan. Deep Sea Res. I 56, 283–293.

Han, X., Suess, E., Sahling, H., Wallman, K., 2004. Fluid venting activity on the Costa Rica margin: new results from authigenic carbonates. Int. J. Earth Sci. 93, 596–611.

Han, X., Suess, E., Huang, Y., Wu, N., Bohrmann, G., Su, X., Eisenhauer, A., Rehder, G., Fang, Y., 2008. Jiulong methane reef: microbial mediation of seep carbonates in the South China Sea. Mar. Geol. 249, 243–256.

Henry, P., Foucher, J.-P., Le Pichon, X., Sibuet, M., Kobayashi, K., Tarits, P., Chamot-Rooke, N., Furuta, T., Schultheiss, P., 1992. Interpretation of temperature measurements from the Kaiko-Nankai cruise: modeling of fluid flow in clam colonies. Earth Planet. Sci. Lett. 109, 355–371.

Henrys, S.A., Ellis, S., Uruski, C., 2003. Conductive heat flow variations from bottom-simulating reflectors on the Hikurangi margin, New Zealand. Geophys. Res. Lett. 30, 1065–1068.

Henrys, S.A., Woodward, D.J., Pecher, I.A., 2010. Variation of bottom-simulating reflection strength in a high-flux methane province, Hikurangi margin, New Zealand. In: Collett, T., Johnson, A., Knapp, C., Boswell, R. (Eds.), Natural Gas Hydrates - Energy Resource Potential and Associated Geologic Hazards. Amer. Assoc. Petrol. Geol. Memoir 89, 481-489.

Hensen, C., Wallman, K., Schmidt, M., Ranero, C.R., Suess, E., 2004. Fluid expulsion related to mud extrusion off Costa Rica—a window to the subducting slab. Geology 32, 201–204.

Hinrichs, K.U., Boetius, A., 2002. The anaerobic oxidation of methane: new insights in microbial ecology and biogeochemistry. In: Wefer, G., Billett, D., Hebbeln, D., Jorgensen, B.B., Schluter, M., Van Weering, T. (Eds.), Ocean Margin Systems. Springer-Verlag, Berlin Heidelberg, pp. 457–477.

Hovland, S.A., Risk, M., 2003. Do Norwegian deep-water coral reefs rely on seeping fluids? Mar. Geol. 198, 83–96.

Irwin, H., Curtis, C., Coleman, M., 1977. Isotopic evidence for source of diagenetic carbonates formed during burial of organic-rich sediments. Nature 269, 209–213.

Jensen, P., Aagaard, I., Burke Jr., R.A., Dando, P.R., Jørgensen, N.O., Kuijpers, A., Laier, T., O'Hara, S.C.M., Schmaljohann, R., 1992. 'Bubbling reefs' in the Kattegat: submarine landscapes of carbonate-cemented rocks support a diverse ecosystem at methane seeps. Mar. Ecol. Prog. Ser. 83, 103–112.

Joye, S.B., Boetius, A., Orcutt, B.N., Montoya, J.P., Schulz, H.N., Erickson, M.J., Lugo, S.K., 2004. The anaerobic oxidation of methane and sulfate reduction in sediments from Gulf of Mexico cold seeps. Chem. Geol. 205, 219–238.

Judd, A.G., Hovland, M., 2007. Seabed Fluid Flow: The Impact on Geology, Biology and the Marine Environment. Cambridge University Press, Cambridge. 475 pp.

Kastner, M., Elderfield, H., Jenkins, W.J., Geiskes, J.M., Gamo, T., 1993. Geochemical and isotopic evidence for fluid flow in the western Nankai subduction zone, Japan. In: Winkler, W., Stewart, N.J. (Eds.), Proc. ODP, Sci. Results vol. 131, pp. 397–413.
Kauffman, E.G., Arthur, M.A., Howe, B., Scholle, P.A., 1996. Widespread venting of methane-rich fluids in Late Cretaceous (Campanian) submarine springs (Tepee Buttes), Western Interior Seaway, U.S.A. Geology 24, 799–802.
Kulm, L.D., Suess, E., 1990. Relationship between carbonate deposits and fluid venting: Oregon accretionary prism. J. Geophys. Res. 95 (B6), 8899–8915.
Levin, L.A., 2005. Ecology of cold seep sediments: interactions of fauna with flow, chemistry, and microbes. Oceanogr. Mar. Biol. Ann. Rev. 43, 1–46.
Levin, L.A., Michener, R.H., 2002. Isotopic evidence for chemosynthesis-based nutrition of macrobenthos: the lightness of being at Pacific methane seeps. Limnol. Oceanogr. 47, 1336–1345.
Lewis, K.B., 1991. Seep faunas and limestone chimneys. N. Z. Prof. Fisherman 4, 16–17.
Lewis, K.B., Marshall, B.A., 1996. Seep faunas and other indicators of methane-rich dewatering on New Zealand convergent margins. N. Z. J. Geol. Geophys. 39, 181–200.
Lewis, K.B., Pettinga, J.R., 1993. The emerging, imbricate frontal wedge of the Hikurangi Margin. In: Ballance, P.F. (Ed.), Sedimentary Basins of the World 2: Basins of the South West Pacific. Elsevier Science Publishers, Amsterdam, pp. 225–250.
Liebetrau, V., Eisenhauer, A., Linke, P., 2010. Cold seep carbonates and associated cold-water corals at the Hikurangi Margin, New Zealand: New insights into fluid pathways, growth structures and geochronology. Mar. Geol. 272, 307–318 (this issue).
Longstaffe, F.J., 1987. Stable isotope studies of diagenetic processes. In: Kyser, T. (Ed.), Short Course in Stable Isotope Geochemistry of Low Temperature Processes: Miner. Soc. Can. Saskatoon, SK, pp. 187–257.
Lowry, D.C., Francis, D.A., Bennett, D.J., 1998. Biogenic gas: a new play in the East Coast Basin of New Zealand. Proc. N. Z. Petrol. Conf, pp. 207–221.
Luff, R., Wallmann, K., Aloisi, G., 2004. Numerical modeling of carbonate crust formation at cold vent sites: significance for fluid and methane budgets and chemosynthetic biological communities. Earth Planet. Sci. Lett. 221, 337–353.
Lyon, G.L., Francis, D.A., Giggenbach, W.F., 1992a. The stable isotope composition of some East Coast natural gases. Proc. N.Z. Oil Expl. Conf, pp. 310–319.
Lyon, G.L., Francis, D.A., Giggenbach, W.F., 1992b. The stable isotope composition of some East Coast natural gases. Proc. N.Z. Oil Expl. Conf, pp. 310–319.
MacDonald, I.R., Boland, G.S., Baker, J.S., Brooks, J.M., Kennicutt II, M.C., Bidigare, R.R., 1989. Gulf of Mexico chemosynthetic communities II. Spatial distribution of seep organisms and hydrocarbons at Bush Hill. Mar. Biol. 101, 235–247.
MacDonald, I.R., Guinasso Jr., N.L., Reilly, J.F., Brooks, J.M., Callender, W.R., Gabrielle, S.G., 1990. Gulf of Mexico hydrocarbon seep communities: VI. Patterns in community structure and habitat. Geo Mar. Lett. 10, 244–252.
Mazzini, A., Duranti, D., Jonk, R., Parnell, J., Cronin, B.T., Hurst, A., Quine, M., 2003. Palaeo-carbonate seep structures above an oil reservoir, Gryphon Field, Tertiary, North Sea. Geo Mar. Lett. 23, 323–339.
Mazzullo, S.J., 2000. Organogenic dolomitization in peritidal to deep-sea sediments. J. Sed. Res. 70, 10–23.
Naehr, T.H., Rodriguez, N.M., Bohrmann, G., Paull, C.K., Botz, R., 2000. Methane-derived authigenic carbonates associated with gas hydrate decomposition and fluid venting above the Blake Ridge Diapir. In: Paull, C.K., Matsumoto, R., Wallace, P.J., Dillon, W.P. (Eds.), Proc. ODP, Sci. Results vol. 164, pp. 285–300.
Naehr, T.H., Eichhubl, P., Orphan, V.J., Hovland, M., Paull, C.K., Ussler III, W., Lorenson, T.D., Greene, H.G., 2007. Authigenic carbonate formation at hydrocarbon seeps in continental margin sediments: a comparative study. Deep-Sea Res. II 54, 1268–1291.
Nelson, C.S., Cochrane, R.H., 1970. A rapid X-ray method for the quantitative determination of selected minerals in fine-grained and altered rocks. Tane 16, 151–162.
Nesbitt, E.A., Campbell, K.A., 2004. Spatial and stratigraphic distribution of fossils from diffuse seeps in a Pliocene shelf setting, Cascadia convergent margin. Geol. Soc. America, Abstr. Prog. 36 (5), 314.
Nyman, S.L., 2009. Tubular carbonate concretions from North Island, New Zealand: Evidence for hydrocarbon migration and the subsurface plumbing system of cold seeps. PhD thesis, University of Waikato, Hamilton, New Zealand.
Nyman, S.L., Nelson, C.S., Campbell, K.A., 2010. Miocene tubular concretions in East Coast Basin, New Zealand: Analogue for the subsurface plumbing of cold seeps. Mar. Geol. 272, 319–336 (this issue).
Olu, K., Sibuet, M., Harmengneis, F., Foucher, J.-P., Fiala-Médioni, A., 1996. Spatial distribution of diverse cold seep communities living on various diapiric structures of the southern Barbados prism. Progr. Oceanogr. 38, 347–376.
Orange, D.L., Greene, H.G., Reed, D., Martin, J.B., McHugh, C.M., Ryan, W.B.F., Maher, N., Stakes, D., Barry, J., 1999. Widespread fluid expulsion on a translated continental margin: mud volcanoes, fault zones, headless canyons, and organic-rich substrate in Monterey Bay, California. Geol. Soc. Amer. Bull. 111, 992–1009.
Orphan, V.J., Ussler III, W., Naehr, T.H., House, C.H., Hinrichs, K.-U., Paull, C.K., 2004. Geological, geochemical, and microbiological heterogeneity of the seafloor around methane vents in the Eel River Basin, offshore California. Chem. Geol. 205, 265–289.
Pancost, R.D., Hopmans, E.C., Sinninghe Damsté, J.S., 2001. Archaeal lipids in Mediterranean cold seeps: molecular proxies for anaerobic methane oxidation. Geochim. Cosmochim. Acta 65, 1611–1627.
Pancost, R.D., Zhang, C.L., Tavacoli, J., Talbot, H.M., Farrimond, P., Schouten, S., Sinninghe Damsté, J.S., Sassen, R., 2005. Lipid biomarkers preserved in hydrate-associated authigenic carbonate rocks of the Gulf of Mexico. Palaeogeogr. Palaeoclimat. Palaeoecol. 227, 48–66.
Paull, C.K., Chanton, J.P., Neumann, A.C., Coston, J.A., Martens, C.S., 1992. Indicators of methane-derived carbonates and chemosynthetic organic carbon deposits: examples from the Florida Escarpment. Palaios 7, 361–375.
Peckmann, J., Reimer, A., Luth, U., Luth, C., Hansen, B.T., Heinicke, C., Hoefs, J., Reitner, J., 2001. Methane-derived carbonates and authigenic pyrite from the northwestern Black Sea. Mar. Geol. 177, 129–150.
Peckmann, J., Birgel, D., Kiel, S., 2009. Molecular fossils reveal fluid composition and flow intensity at a Cretaceous seep. Geology 37, 847–850.
Ritger, S., Carson, B., Suess, E., 1987. Methane-derived authigenic carbonates formed by subduction-induced pore-water expulsion along the Oregon/Washington margin. Geol. Soc. Amer. Bull. 98, 147–156.
Roberts, H.H., Aharon, P., 1994. Hydrocarbon-derived carbonate buildups of the northern Gulf of Mexico: a review of submersible investigations. Geo Mar. Lett. 14, 135–148.
Sahling, H., Rickert, D., Lee, R.W., Linke, P., Suess, E., 2002. Macrofaunal community structure and sulphide flux at gas hydrate deposits from the Cascadia convergent margin, NE Pacific. Mar. Ecol. Prog. Ser. 231, 121–138.
Sahling, H., Galkin, S.V., Salyuk, A., Greinert, J., Foerstel, H., Piepenburg, D., Suess, E., 2003. Depth-related structure and ecological significance of cold-seep communities — a case study from the Sea of Okhotsk. Deep Sea Res. I 50, 1391–1409.
Sakai, H., Gamo, T., Ogawa, Y., Boulegue, J., 1992. Stable isotopic ratios and origins of the carbonates associated with cold seepage at the eastern Nankai Trough. Earth Planet. Sci. Lett. 109, 391–404.
Sassen, R., MacDonald, I., 1998. Bacterial methane oxidation in sea-floor gas hydrate: significance to life in extreme environments. Geology 26, 851–854.
Sassen, R., Roberts, H.H., Carney, R., Milkov, A.V., DeFreitas, D.A., Lanoil, B., Zhang, C., 2004. Free hydrocarbon gas, gas hydrate, and authigenic minerals in chemosynthetic communities of the northern Gulf of Mexico continental slope: relation to microbial processes. Chem. Geol. 205, 195–217.
Savard, M.M., Beauchamp, B., Veizer, J., 1996. Significance of aragonite cements around Cretaceous marine methane seeps. J. Sed. Res. 66, 430–438.
Seilacher, A., 1990. Aberrations in bivalve evolution related to photo- and chemosymbiosis. Hist. Biol. 3, 289–311.
Sellanes, J., Quiroga, E., Neira, C., 2008. Megafauna community structure and trophic relationships at the recently discovered Concepción methane seep area, Chile, 36°S. J. Mar. Sci. 65, 1102–1111.
Shapiro, R.S., 2004. Recognition of fossil prokaryotes in Cretaceous methane seep carbonates: relevance to astrobiology. Astrobiology 4, 438–449.
Sibson, R.H., 1994. Crustal stress, faulting and fluid flow. In Parnell J. (ed). Geofluids: Origin, Migration and Evolution of Fluids in Sedimentary Basins. Geol. Soc. Spec. Pub. 78, 69–84.
Sibson, R.H., Rowland, J.V., 2003. Stress, fluid pressure and structural permeability in seismogenic crust, North Island, New Zealand. Geophys. J. Int. 154, 584–594.
Sibuet, M., Olu, K., 1998. Biogeography, biodiversity and fluid dependence of deep-sea cold-seep communities at active and passive margins. Deep Sea Res. II 45, 517–567.
Sibuet, M., Juniper, S.K., Pautot, G., 1988. Cold-seep benthic communities in the Japan subduction zones: geological control of community development. J. Mar. Res. 46, 333–348.
Sommer, S., Pfannkuche, O., Linke, P., Luff, R., Greinert, J., Drews, M., Gubsch, S., Pieper, M., Poser, M., Viergutz, T., 2006. Efficiency of the benthic filter: biological control of the emission of dissolved methane from sediments containing shallow gas hydrates at Hydrate Ridge. Global Biogeochem. Cycles 20, GB2019. doi:10.1029/2004GB002389.
Stakes, D.S., Orange, D., Paduan, J.B., Salamy, K.A., Maher, N., 1999. Cold-seeps and authigenic carbonate formation in Monterey Bay, California. Mar. Geol. 159, 93–109.
Suess, E., Whiticar, M.J., 1989. Methane-derived CO_2 in pore fluids expelled from the Oregon subduction zone. Palaeogeogr. Palaeoclimat. Palaeoecol. 71, 119–136.
Suess, E., Bohrmann, G., von Huene, R., Linke, P., Wallmann, K., Lammers, S., Sahling, H., 1998. Fluid venting in the eastern Aleutian subduction zone. J. Geophys. Res. 103 (B2), 2597–2614.
Svensen, H., Planke, S., Jamtveit, B., Pederson, T., 2003. Seep carbonate formation controlled by hydrothermal vent complexes: a case study from the Vøring Basin, the Norwegian Sea. Geo Mar. Lett. 23, 351–358.
Tap Oil Ltd, 2004. Tawatawa-1 well completion report vol. 3067. Petroleum Report. 873 pp.
Teichert, B.M.A., Gussone, N., Eisenhauer, A., Bohrmann, G., 2005a. Clathrites: archives of near-seafloor pore-fluid evolution ($\delta^{44/40}$Ca, δ^{13}C, δ^{18}O) in gas hydrate environments. Geology 33, 213–216.
Teichert, B.M.A., Bohrmann, G., Suess, E., 2005b. Chemoherms on Hydrate Ridge — unique microbially-mediated carbonate build-ups growing into the water column. Palaeogeogr. Palaeoclimat. Palaeoecol. 227, 67–85.
Thiel, V., Peckmann, J., Richnow, H.H., Luth, U., Reitner, J., Michaelis, W., 2001. Molecular signals for anaerobic methane oxidation in Black Sea seep carbonates and a microbial mat. Mar. Chem. 73, 97–112.
Thurber, A.R., Kröger, K., Neira, C., Wiklund, H., Levin, L.A., 2010. Stable isotope signatures and methane use by New Zealand cold seep benthos. Mar. Geol. 272, 260–269 (this issue).
Treude, T., Boetius, A., Knittel, K., Wallmann, K., Jorgensen, B.B., 2003. Anaerobic oxidation of methane above gas hydrates at Hydrate Ridge, N.E. Pacific Ocean. Mar. Ecol. Prog. Ser. 264, 1–14.
Tryon, M.D., Brown, K.M., Torres, M.E., 2002. Fluid and chemical flux in and out of sediments hosting methane hydrate deposits on Hydrate Ridge, OR, II: hydrological processes. Earth Planet. Sci. Lett. 201, 541–557.
Ussler III, W., Paull, C.K., 1995. Effects of ion exclusion and isotopic fractionation on pore water geochemistry during gas hydrate formation and decomposition. Geo Mar. Lett. 15, 37–44.
Van Dover, C.L., 2000. The Ecology of Deep-Sea Hydrothermal Vents. Princeton University Press, Princeton, New Jersey. 424 pp.
Van Dover, C.L., Aharon, P., Bernhard, J.M., Caylor, E., Doerries, M., Flickinger, W., Gilhooly, W., Goffredi, S.K., Knick, K.E., Macko, S.A., Rapoport, S., Raulfs, E.C., Ruppel, C., Salerno, J.L., Seitz, R.D., Sen Gupta, B.K., Shank, T., Turnipseed, M., Vrijenhoek, R., 2003. Blake Ridge methane seeps: characterization of a soft-sediment, chemosynthetically based ecosystem. Deep Sea Res. I 50, 281–300.

Volkman, J.K., 1986. A review of sterol markers for marine and terrigenous organic matter. Org. Geochem. 9, 83–99.
Volkman, J.K., Barrett, S.M., Blackburn, S.I., Mansour, M.P., Sikes, E.L., Gelin, F., 1998. Microalgal biomarkers: a review of recent research developments. Org. Geochem. 29, 1163–1179.
von Rad, U., Rösch, H., Berner, U., Geyh, M., Marchig, V., Schulz, H., 1996. Authigenic carbonates from oxidized methane vented from the Makah accretionary prism off Pakistan. Mar. Geol. 136, 55–77.
Vrolijk, P., 1993. On the mechanical role of smectite in subduction zones. Geology 18, 703–707.
Wallmann, K., Linke, P., Suess, E., Bohrmann, G., Sahling, H., Schlüter, M., Dählmann, A., Lammers, S., Greinert, J., von Mirbach, N., 1997. Quantifying fluid flow, solute mixing, and biogeochemical turnover at cold vents of the eastern Aleutian subduction zone. Geochim. Cosmochim. Acta 61, 5209–5219.
Whiticar, M.J., 1999. Carbon and hydrogen isotope systematics of bacterial formation and oxidation of methane. Chem. Geol. 161, 291–314.
Williams, D.F., Trainor, D.M., 1987. Carbon isotope signals for chemical stratigraphy and hydrocarbon exploration in the northern Gulf of Mexico. Gulf Coast Assoc. Geol. Soc. Trans. 37, 287–294.